Aalto University
School of Engineering

Chiara Ghio

Transport of fine sediment in vegetated flows

Master's thesis for the degree of Master of Science in Technology submitted for inspection

Espoo, 20.07.2018
Supervisors: Prof. Harri Koivusalo, Prof. Davide Poggi
Advisors: Dr. Juha Järvelä, Dr. Kaisa Västilä

Aalto University
School of Engineering

Aalto University, P.O. BOX 11000, 00076 AALTO
www.aalto.fi

Abstract of master's thesis

Author Chiara Ghio

Title of thesis Transport of fine sediment in vegetated flows

Master programme Water and Environmental Engineering **Code** R3005

Thesis supervisor(s) Prof. Harri Koivusalo, Prof. Davide Poggi

Thesis advisor(s) Dr. Juha Järvelä, Dr. Kaisa Västilä

Date 20.07.2018 **Number of pages** 67 **Language** English

Abstract

Complex interactions and turbulent flow structures take place across the interface, between vegetated regions and unobstructed main channel flow. For instance, in partly vegetated flows, different transport processes and sediment deposition affect the availability of nutrients and presence of pollutants. Within the vegetation, the turbidity is altered, influencing light accessibility and photosynthesis. The goal of this thesis is to improve knowledge on turbulent flow and fine sediment transport in partly vegetated flows. Experiments were carried out in the Aalto Environmental Hydraulics Lab:~60% of the flume width was unvegetated, while ~40% of the flume width was covered by a vegetated patch comprised of understory grass mat and artificial emergent flexible natural-like plants.

The experiments used a combination of vegetation density and plant properties, well representative of conditions found in natural riverine flows. Instantaneous 3D velocities, suspended sediment concentration (SSC) and net deposition were measured in the fully developed flow region of the vegetated patch. Two transverse transects and several vertical profiles were measured. Two vegetation conditions, representing the seasonal changes due to lifecycle of riverine plants, were investigated: leafless and foliated. In addition to descriptive data analyses, equations from literature were applied and tested against the flume measurements to check if it was possible to use them for a reliable prediction under the examined vegetative conditions.

The experimental data showed that effects of the presence of vegetation on flow field and fine sediment transport vary when the plant density increases (i.e. changing from leafless to foliated condition). The difference in streamwise velocity between the open channel and the vegetated region increased. SSC decreased, within the foliated vegetation compared to the main channel, in agreement with the decrease in velocity and increase in net deposition. Under foliated condition, the mechanical dispersion appeared to lead sediment transport, because turbulence declined rapidly. In the leafless case, the turbulence at the stem scale was the main player, determining high local fluctuations in transversal and vertical profiles for both SSC and streamwise velocity and a reduction in net deposition. Overall, the investigations on flow-vegetation-sediment processes performed in two different conditions, representing seasonal vegetation changes, showed that theoretical and empirical relationships used to predict patterns of velocity are less suitable for predictions within leafy vegetation, but they still are in good agreement within flows in leafless condition. For SSC patterns, the predictions through equations and assumptions used in unvegetated channel are hard to obtain and unreliable in both vegetative conditions.

Keywords Partly vegetated flow, Fine sediment, Suspended sediment, Net deposition, Flow field, Emergent vegetation.

Acknowledgements

This study complemented an ongoing research project entitled "*Controlling transport of nutrients by means of environmental two-stage channels*" funded by Maa-ja Vesitekniikan Tuki. The main core of the project is improving quality of surface waters through managing sediment and nutrient processes. The experiments have been carried out in the Environmental Hydraulics Lab in Aalto University, in collaboration of the experiments held by the doctoral candidate Walter Box, to whom I express my profound gratitude for helping me during measurements and solving my doubts during data processing. All data presented within this thesis is part of a larger dataset which will be published later in the afore mentioned project.

I would like to thank Professors Harri Koivusalo and Davide Poggi, who supervised my thesis, and my advisors Dr. Juha Järvelä and Dr. Kaisa Västilä for insights, useful guidance and feedback they have given to me in the development of this work. Moreover, I gratefully acknowledge the help of laboratory technician Antti Louhio and PhD student Gerardo Caroppi for preliminary work done on the used artificial vegetation and, especially, Gerardo for his hints and technical guidance on the software Velocity Signal Analyzer (VSA).

It is my duty to thank my family: my parents Luigi and Mirella who have supported me and give me the possibility to follow my passions and go abroad as an exchange student, my sister Valeria and my two brothers Filippo and Simone who always encouraged me and supported me in my choices.

I cannot forget to thank my flatmates Nadin and Olek, for listening to me and being an indispensable moral support in stressful periods, and my friends Lucia, Michela and Arianna who, despite the distance, have been always present knowing how to, positively, stimulate me.

Finally, I would like to express my sincere gratitude to all people encountered in these five academic years. In particular, a special mention for all my friends met in the Erasmus period and in the Alta Scuola Politecnica (ASP).

Helsinki, 18.07.2018

Chiara Ghio

Table of contents

List of symbols

a	Frontal area per unit of water volume (m^{-1})
a_L	Frontal area of leaves per unit of water volume (m^{-1})
a_S	Stem frontal area per unit of water volume (m^{-1})
A_B	Bed area (m^2)
A_f	Characteristic frontal area (m^2)
A_L	Frontal area of leaves (m^2)
A_S	Stem frontal area (m^2)
b	Width of the vegetated patch (m)
B	Width of the channel (m)
Bio	Biomechanical parameter of vegetation (-)
c	Integration constant of the log law formula (-)
C	Sediment concentration (kg/l)
C_α	Reference concentration at height α above the bed (kg/l)
C_C	Gradation coefficient (-)
C_D	Drag coefficient (-)
$C_{D_{\chi,F}}$	Drag coefficient for the foliage, function of the reconfiguration χ (-)
$C_{D_{\chi,S}}$	Drag coefficient for the stem, function of the reconfiguration χ (-)
$C_D a$	Drag-density parameter (m^{-1})
$C_D ah$	Drag-area parameter (-)
c_f	Bed friction coefficient (-)
C_L	Lift coefficient (-)
C_U	Uniformity coefficient (-)
C_1	Arbitrary threshold parameter (-)
C_2	Empirical constant (-)
d	Characteristic stem diameter (m)
d_p	Particle diameter (m)
d_*	Dimensionless particle diameter (-)
d_{10}	Size of the sieve with 10% finer sediments passing (m)
d_{30}	Size of the sieve with 30% finer sediments passing (m)
d_{50}	Median particle diameter (m)
d_{60}	Size of the sieve with 60% finer sediments passing (m)
D_m	Molecular diffusion (m^2/s)
E	Young's modulus (N/m^2)
f''	Vegetative friction factor (-)
F_D	Drag force (N)
F_F	Leaves drag force (N)
F_L	Lift force (N)
Fr	Froude number (-)
F_S	Stem drag force (N)
g	Gravitational acceleration (m/s^2)
Δs	Stem spacing (m)
h or H	Canopy height or water depth since in this study they are equal (m)
K	Volumetric shape factor (-)
k_s	Equivalent sand roughness (m)
I	Turbulence intensity (-)
I_2	Second moment of cross sectional area (m^4)

m	Number of stems per bed area (m^{-2})
n	Number of data points (-)
n_c	Manning coefficient (-)
n_{veg}	Vegetative Manning coefficient (-)
p	Pressure (N/m^2)
P	Probability that a particle reaching the bed will not be re-suspended again (-)
Q	Discharge (m^3/s)
r_{dep}	Rate of net deposition (kg/s)
r_{depmax}	Maximum rate of net deposition (kg/s)
Re_h	Reynolds number linked to the flow depth (-)
Re_p	Particle Reynolds number (-)
Re_δ	Reynolds number linked to the momentum thickness (-)
Re_{xy}	Lateral Reynolds stress (N/m^2)
Re_{xymax}	Maximum lateral Reynolds stress (N/m^2)
Re_{xz}	Vertical Reynolds stress (N/m^2)
Re_{xzmax}	Maximum vertical Reynolds stress (N/m^2)
R_s	Spacing hydraulic radius (m)
RMS	Root Mean Square relative error (%)
S	Bottom slope (%)
S_f	Friction slope (%)
t	Time (s)
TKE	Turbulent kinetic energy (m^2/s^2)
U	Velocity magnitude (m/s)
U_m	Streamwise velocity observed at y_m (m/s)
$\langle U \rangle_{max}$	Maximum streamwise velocity along the cross-section (m/s)
U_s	Slip velocity (m/s)
U_1	Uniform streamwise velocity within the patch (m/s)
U_2	Uniform streamwise velocity in the open-channel (m/s)
$U_{\chi,F}$	Reference velocity for foliage used to calculate the reconfiguration parameter χ_F (m/s)
$U_{\chi,S}$	Reference velocity for stem used to calculate the reconfiguration parameter χ_S (m/s)
u	Instantaneous streamwise velocity (m/s)
u'	Velocity fluctuation in x direction (m/s)
u_m	Expected maximum value (m/s)
u_{max}	Maximum streamwise velocity along the vertical profile (m/s)
u_*	Shear velocity (m/s)
v	Instantaneous transverse velocity (m/s)
v'	Velocity fluctuation in y direction (m/s)
V_{SSC}	Suspended sediment concentration (Voltage)
V_{SSCmax}	Maximum suspended sediment concentration (Voltage)
V_{SSCref}	Reference suspended sediment concentration (Voltage)
w	Instantaneous vertical velocity (m/s)
w'	Velocity fluctuation in z direction (m/s)
w_s	Particle settling velocity (m/s)
w_{ss}	Settling velocity for a spherical particle (m/s)
x	Axis in streamwise direction (m)

x_a	Advection length (m)
x_D	Diverging length (m)
x_o	Observed value
x_e	Estimated value
y	Axis in transverse direction (m)
y_m	Location in which the inner and outer layer slopes match (m)
y_0	Location in which the lateral Reynolds stress is maximum (m)
z	Axis in vertical direction (m)
z_0	Hydrodynamic roughness length (m)
α	Reference height (m)
δ	Thickness of the mixing shear layer (m)
δ_I	Thickness of inner layer (m)
δ_O	Thickness of outer layer (m)
ε_y	Sediment diffusivity coefficients in the transverse direction (m^2/s)
ε_z	Sediment diffusivity in the vertical direction (m^2/s)
θ_u	Median absolute deviation of the velocity time series (m/s)
κ	Von Karman constant (-)
λ	Frontal area per bed area (m^2/m^2)
μ	Dynamic viscosity (Ns/m^2)
ρ	Water density (kg/m^3)
ρ_v	Canopy density (kg/m^3)
ρ_p	Particle density (kg/m^3)
σ	Standard deviation
τ	Total shear stress (N/m^2)
τ_b	Bed-shear stress (N/m^2)
τ_v	Shear stress due to the vegetation (N/m^2)
τ_{xy}	Lateral shear stress (N/m^2)
τ_{xz}	Vertical shear stress (N/m^2)
v	Kinematic viscosity (m^2/s)
ξ	Shape factor of a solid particle (-)
φ	Canopy porosity (-)
ϕ	Solid volume fraction occupied by the individual plant (-)
χ	Vogel exponent or reconfiguration parameter (-)
χ_F	Reconfiguration parameter for foliage (-)
χ_S	Reconfiguration parameter for stem (-)

List of Figures

List of Tables

1. Introduction

Aquatic ecosystem and biodiversity take part in a fragile balance strictly interlinked to different factors such as water flow, presence of nutrients and oxygen, and characteristics of the riverine vegetation. Often, behaviour of organisms and their life style are influenced by transport processes; for example, some aquatic organisms used advection and dispersion processes for foraging or transport of their larval stages (e.g. Lightbody & Nepf, 2006). When nutrients and oxygen, moving with the water flow, enter the thin diffusive boundary layer present around vegetation, they can be uptaken by the plants. Usually, due to the purification role of the vegetation, water quality is enhanced; indeed, pollutants, trapped or absorbed on surface of fine sediments, are transported with the water flow and experience, when they encounter vegetated patches, phenomena such as absorption, sedimentation, and microbial transformation. Riverine plants decrease suspended solids concentration, sequestering heavy metals (e.g. arsenic, mercury, lead) on surface of particles, reducing turbidity and consequently increasing light availability and photosynthesis. On the other hand, aquatic vegetation tends to reduce flow velocity field and determine sediment deposition, ensuring good conditions for subsistence and growth of new biomass. The latter phenomenon is strictly linked to planimetric changes of river flow meanderings due to vegetation presence (e.g. Bennett et al., 2002).

The first studies related to riverine vegetation were focused just on the hydraulic perspective, considering vegetation as flow resistance, because it is regarded as the main cause of the reduction of the water flow velocity. The ecological point of view, together with physics, chemistry and biology, should not be forgotten, because it considers plants as integral part of the aquatic ecosystem (Järvelä, 2002). An enhanced interdisciplinary characterization of flow structure and transport processes, taking into account all the interactions and the complexity of the problem, is needed. For example, riverine vegetation includes different types of species spatially and irregularly distributed and river and channel flow regimes exist in a wide range of different forms, from small mountain streams and agricultural channel to large rivers (Folkard, 2011). In addition, effects of presence of vegetation can be observed at different scales. For instance, nutrient uptake is governed by individual plants at the blade-scale flow; whereas, sediment retention in a vegetated patch can be studied by focusing on patch-scale or reach-scale flow (e.g. Nepf, 2012b).

Accurate results and predictions of flow-vegetation processes have been and are still achieved by using adequate measuring techniques in field campaigns and laboratory experiments, and reliable tools for analysis. This is the way to develop practical management techniques for water quality issues and maintenance. For instance, recent practices such as soil bioengineering, combines methods using plants with conventional measurements, facing problems of bank stabilization and erosion (e.g. Västilä & Järvelä, 2017). High suspended particle loads can alter the morphology and habitats in riverine

ecosystem, increasing turbidity and affecting the water quality and the benthic and aquatic biota.

Overall, flow-vegetation-sediment interactions are not fully understood as long as the biunivocal interconnection between biomechanical/morphological properties of aquatic vegetation and flow dynamics properties remains unclear (e.g. Nikora, 2010). Variation in flow dynamics can change vegetation characteristics (e.g. reconfiguration); at the same time, changes in relative plant height (e.g. shift between submerged and emergent vegetation) affect the hydraulic characteristics of the water flow.

1.1 Goal and focus of this study

The scope of this study is to improve knowledge on flow fields and transport processes in vegetated flows, collecting new data by laboratory experiments in the Aalto Environmental Hydraulics Flume. This thesis complements an ongoing doctoral research project with the intention to improve quality of surface water through managing sediment and nutrient processes. The specific objectives can be summarized as follows:

1. To characterize flow fields in a partially vegetated channel with natural-like flexible plants;
2. To characterize transport of suspend fine sediment in a partially vegetated flow through turbidity measurements;
3. To describe net deposition of fine sediment within a vegetated patch.

To achieve these goals, a partly vegetated channel was reconstructed within the hydraulic flume. The artificial vegetation consisted of emergent woody plants with an understory of dense flexible grass, in two conditions: leafless and foliated. Their morphology and dynamics in the water flow represent the behaviour of natural plants against the water flow (i.e. reconfiguration of stems and leaves under the water flow). Discharge, water level and sediment feeding rate remained constant for the experiments. The measurements were focused on the fully developed flow region, adjusting boundary conditions to have steady uniform flow for the entire working section of the flume.

Finally, selected applicability tests of theoretical and empirical equations were carried out in order to see how large deviations or similarities are. Commonly, models defined initially for unvegetated flow, are used to characterize flow field and sediment transport in vegetated channels. Parameters affected by the presence of the vegetation such as flow resistance, bed stress, are obtained through new formulations.

2. Flow and sediment transport in vegetated channels: literature review

2.1 Characteristics of riverine vegetation

Vegetation placed along rivers and channels or in the riparian zone can be classified, according to species and foliage, to aquatic plants, grass, shrubs and woody trees. Aquatic plants (*Figure 2.1*) are usually under water or floating in river channels; whereas grass and shrubs can be submerged or emergent and they are characteristic of river banks or floodplains. Grass is composed by single leafless, rigid or flexible, stems and it exhibits usually high density; while, shrubs are bushy species with stems and leaves, characterized by different foliage density (Vargas-Luna et al., 2015; Aberle & Järvelä, 2015). The riparian zone[1] generally includes woody vegetation such as rigid or flexible woody trees and bushes.

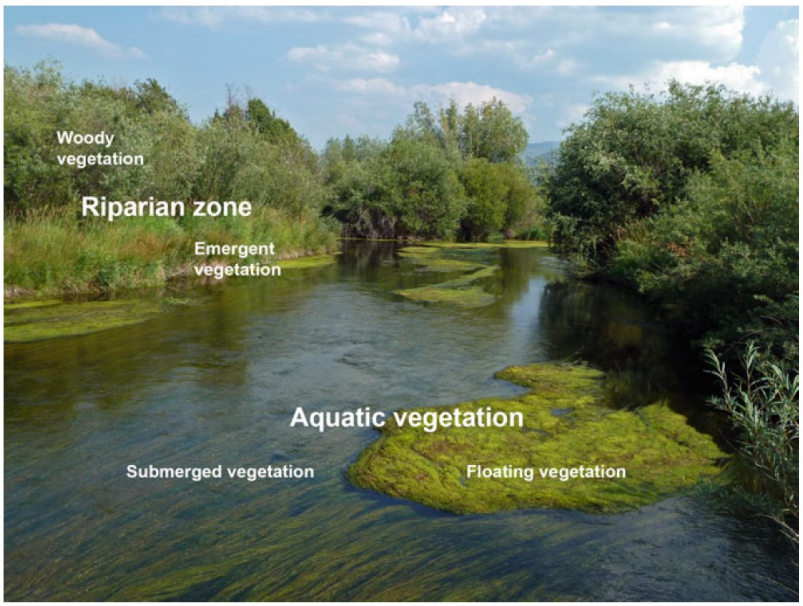

Figure 2.1: Classification of vegetation that can be found in rivers/channels and in the riparian zone (Aberle & Järvelä, 2015).

Due to different vegetation types, biological, chemical and mechanical properties contribute to alter the water flow in different ways (e.g. Kouwen, 1998). Forces such as tension, compression, bending torsion and shear are strictly linked with flow and plant interaction (e.g. Nikora, 2010). For this reason, knowing the vegetation parameterization is fundamental in order to fully understand phenomena taking place in rivers or channels. According to the scale defined, different level of complexity is needed. The selection of approaches and variables varies from leaf scale to, zooming out, shoot[2] scale, individual

[1] Transition zone between aquatic and terrestrial ecosystem.
[2] Stem including its appendages such as leaves and flowers.

plant (sum of shoots) scale, patch[3] scale, reach and mosaic[4] scale and, finally, to the whole-river scale (e.g. Aberle & Järvelä, 2015; Nikora, 2010).

2.1.1 Plant morphology

At the canopy scale, aquatic plants have a visual structure that can be described in terms of linear, areal, and volumetric geometries. In the majority of studies (e.g. Plew, 2011; Poggi et al., 2004; Zong & Nepf, 2010; White & Nepf, 2008), the natural plant was described using rigid or flexible cylinders. This 3D solid is easy to characterize, knowing its height and characteristic diameter. Considering the disposition of these cylinders among each other (spacing), the frontal area per unit of water volume can be obtained through:

$$a = \frac{d}{(\Delta s)^2} \qquad (1)$$

where a is the frontal area per unit of water volume (m^{-1}), d is the characteristic stem diameter (m) and Δs is the stem spacing (m). A non-dimensional canopy density can be defined by different variables: as the frontal area per bed area (λ), as the solid volume fraction occupied by the individual plant (ϕ), or as the canopy porosity[5] (φ). Their formulations and some of their values for particular characteristic diameter and frontal area per unit of water volume can be found in literature, if the vegetation considered has cylinder-like shape (e.g. Nepf, 2012a; Luhar et al., 2008).

In the cylinder simplification, one of the three dimension, such as the plant width, is missing. A more realistic representation is given considering the plant as a structure, including stem, branches and leaves, rather than a simple material (Nikora, 2010). Each vegetation element plays an important role in the interaction with the water flow and in the development of turbulent effects at different scales. As Jalonen et al. (2013; 2014) suggested, the characteristic frontal project area (A_f) of the plant can be determined measuring the *leaf area index*[6] (LAI) through different methods (e.g. remote sensing, laser scanning and image analysis), taking into account the parametrization of leaves and seasonal variations in morphologic variables. Life cycle of deciduous plants is characterized by a growth season, where in the determination of the frontal project area there is the addiction of the presence of leaves (A_L), and autumn-winter period, where just bare branches (A_S) generate resistance to the flow. In winter, cylinder-shape simplification can be representative for woody deciduous plant and its parametrization is suitable. The *frontal area index*, in this case, can be calculated by multiplying the stem frontal area for the number of stems that the canopy contains per unit of bed area:

[3] Small area including plants.
[4] Area characterized by aggregation of patches.
[5] Solid volume fraction not covered by vegetation ($\varphi = 1 - \phi$).

[6] Defines the measurements of one-sided green leaf area per unit of the ground area.

$$ah = mA_f \quad (2)$$

where h is the canopy height (m) and m is the number of stems per bed area (m^{-2}).

2.1.2 Plant biomechanical properties

Previous studies (e.g. Kouwen, 1998; Nepf, 2012a) parameterized plants by their density (ρ_v), Young's (elasticity) modulus[7] (E) and second moment of cross sectional area[8] (I_2). These properties were determined through, for example, uniaxial tension tests, uniaxial cycling loading/unloading and bending tests (e.g. Miler et al., 2014; Łoboda et al., 2018). The plant density is influenced by the gravity force and the buoyancy force, strictly related to the submerged weight of the plant. E and I_2 are, usually, multiplied together in order to obtain the so called *flexural rigidity* (EI_2) describing resistance of an object during its deformation. According to Nikora (2010), when EI_2 is very low, plants are tensile and experience mostly the viscous drag, following passively the flow. When EI_2 is high, bending plants resist to the flow, generating pressure drag. When EI_2 is multiplied by the number of stems per bed area, the aggregate stiffness (mEI_2) can be determined for predicting any kind of canopy motion under the water flow (Nezu & Okamoto, 2013). According to biomechanical properties, the aquatic vegetation can be divided in four categories: 1) erect or rigid plants that do not change their tip position in time, 2) swaying plants that wave without organized motion, 3) monami plants that give well-organized response to coherent vortices (Ghisalberti & Nepf, 2002) and 4) prone plants which exist under large drag force. Kouwen and Unny (1973) proposed a parameter (Bio) able to distinguish between rigid plants (high value of Bio) and prone ones (low value of Bio). This parameter can be derived through:

$$Bio = \left(\frac{mEI_2}{\rho u_*^2}\right)^{1/4} \quad (3)$$

where u_* is the friction velocity (m/s) and ρ is the water density (kg/m^3). The flexural rigidity of an individual grass blade is difficult to determine and it has a high variability. For example, variation of E can be of up to 100% for different samples (Wilson, 2007). Moreover, plant behaviour varies depending on seasons and stage of growth. Dormant or growth stages result in different effects as found out by Albayrak et al. (2014): younger leaves exhibit appreciably lower drag force variability than older ones, because they are more flexible. Also, biomechanics in stem and leaves is different and can produce altered drag force and turbulence next to, over and within the vegetation. On one hand, leaves are flexural structures, playing an important role at the leaf scale and generating a specific resistance force (F_F). On the other hand, they allow a better reconfiguration, that is explained by a decrease in the stem drag (F_S) at low velocities (Aberle & Järvelä, 2015).

[7] Estimation of the stem stiffness under bending forces orthogonal to the canopy.
[8] Estimation on the efficiency of the bending resistance generated by a loading.

Plants cannot be considered as conventional obstruction due to the interaction between the drag force and the restoring force coming from the stem stiffness (e.g. Siniscalchi et al., 2012). When the velocity of the water flow changes, the reconfiguration of the vegetation under the flow varies accordingly. For example, if the flow velocity increases, the frontal project area decreases with the consequent reduction of the drag force (F_D) (see *Equation 5*). According to Aberle & Järvelä (2015) and Luhar & Nepf (2011), the drag force does not vary following the quadratic law of the reference flow velocity (U^2) (*Equation 5*). The increasing rate of the drag force with the velocity is lower than the one obtained for rigid cylinders, as noticed by Västilä & Järvelä (2017) for foliated plants. A non-quadratic relationship, expressed generally in literature as $U^{2+\chi}$, where χ is the *Vogel exponent* or *reconfiguration parameter*, describes better the role of the reconfiguration. The Vogel exponent value is usually below zero for flexible plants, so that the velocity of the water flow has a lower impact on the drag force. χ becomes zero for rigid elements and the drag force varies again following the quadratic law.

2.2 Influence of vegetation on the flow field and resistance

The flow field and the bed shear stress are strongly affected by different area of extent of vegetation along the water depth. Three different types of vegetation (*Figure 2.2*) are commonly determined, according to their relative depth in the water flow: submerged, emergent and suspended or floating. Submerged plants grow completely under the water level; emergent plants have part of the stem under the water surface, covering the full depth of the water flow; suspended vegetation floats near the free water surface and it is not anchored to the substrate surface by roots. In the characterization of the flow field, each type of vegetation generates its own vertical velocity profiles (Plew, 2011).

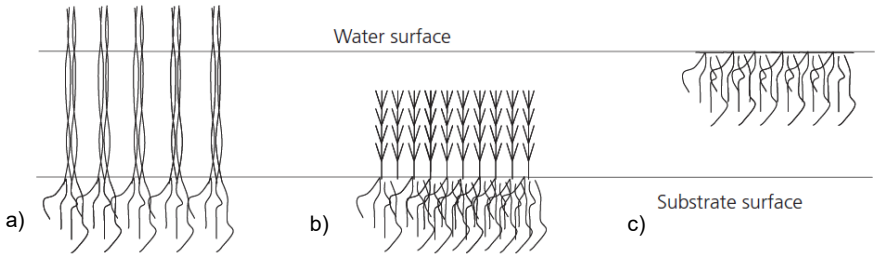

Figure 2.2: Configuration of riverine vegetation along the water flow: a) emergent vegetation, b) submerged vegetation, c) floating or suspended vegetation. (Modified from Folkard 2011)

Vegetation is identified as a cause of flow resistance, depending on plant morphology (*Section 2.1.1*), flexibility (*Section 2.1.2*) and distribution. In natural channel, the distribution of vegetation is random and each cross-section has different shape and percentage of vegetation presence. According to Bal et al. (2011) and Luhar & Nepf (2013), higher variation of flow resistance is detected at interfacial edges between vegetated and unvegetated areas. Hence, the flow resistance can differ depending on the cross-section considered. In laboratory experiments (e.g. Luhar et al., 2008; Sharpe &

James, 2006; Zong & Nepf, 2010), the variation in the vegetation distribution in partly vegetated channel is simplified as shown in *Figure 2.3*. The shape of the cross-section is rectangular with constant area BxH, where B is the width of the flume and H is the water depth. The random vegetation distribution is described by a representative average vegetation density located in a long rectangular strip along one side of the flume, characterized by a plant height (h) and a patch width (b).

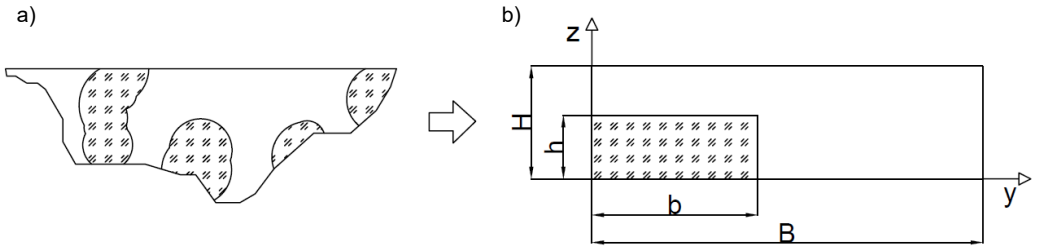

Figure 2.3: Cross-section of a partially vegetated channel: a) natural conditions, b) simplified model in laboratory experiments.

2.2.1 Vegetation as flow resistance

In vegetated channels, the total shear stress (τ) is a linear superposition of the bed-shear stress (τ_b) and the shear stress due to the vegetation (τ_v) (Vargas-Luna et al., 2015; Västilä, 2015):

$$\tau = \tau_b + \tau_v \qquad (4)$$

The resistance to the flow due to the presence of boundary roughness, channel geometry and obstructions, is enhanced by vegetation because of variation in pressure and viscosity around plants and at the interface between vegetated and unvegetated areas. In addition, literature suggests that, within vegetated patches, the main contribution to the drag is due to the vegetation. For example, Västilä et al. (2016) obtained in a field experiment that an average of 89% in the contribution of the total resistance was due to the presence of the vegetation. The value of the bed resistance can be negligible within patches (e.g. Luhar et al., 2008; Nepf, 1999). Unlike open-channel flows, the turbulence production cannot be predicted just considering the bed shear and the turbulence generated by the presence of plants has to be taken into account (Nepf et al., 2013).

The forces governing water flow in vegetated channels are drag (F_D) and lift (F_L) forces, describing by their dimensionless coefficients: the drag coefficient (C_D) and the lift coefficient (C_L), respectively (Aberle & Järvelä, 2015). The drag force is usually defined as:

$$F_D = \frac{1}{2}\rho C_D A_f {U_1}^2 \qquad (5)$$

where U_1 is the cross-sectional average velocity within the vegetation (m/s). This quadratic law depends on plant properties (*Section 2.1.2*) and it does not describe the complexity of effects due to vegetation reconfiguration. Therefore, other formulations, listed by Aberle & Järvelä (2015), have to be taken into account. Experiments conducted by Dunn et al. (1996) with rigid rod-like elements in an open channel, showed that C_D does not have a constant vertical profile, but it increases reaching its maximum at a distance of one third of the vegetation element height above the bed. However, the drag coefficient is usually assumed as a constant, taking into account its average value (Lopez & Garcia, 1998), and it is supposed equal to the unity, if the vegetation behaves as rigid cylinders (Västilä & Järvelä, 2017). For flexible vegetation, it can be estimated from the *momentum balance* (*Section 2.2.2*), considering a uniform and steady state flow. This simplification formulates as a balance between the total drag and the pressure gradient due to the free surface slope, assuming the bed roughness is negligible, through (White & Nepf, 2008):

$$\frac{1}{2} C_D a {U_1}^2 = -g \frac{dh}{dx} \qquad (6)$$

where g is the gravitational acceleration (m/s^2) and $\frac{dh}{dx}$ is the free surface gradient (m/m).

Other common formulations describing the vegetation resistance are summarized by Västilä & Järvelä (2017). The formulations can be used to describe seasonal changes in vegetation morphology (foliated, leafless), due to the distinction between leaves and stem in the parametrization of the vegetation. The flow resistance can be defined as drag-density parameter ($C_D a$), drag-area parameter ($C_D ah$), vegetative friction factor (f'') and vegetative Manning coefficient (n_{veg}). $C_D a$ defines the vegetative drag per unit of water volume and it is related to *Equation 5*; for foliated woody plants, it can be calculated through (Västilä & Järvelä, 2017):

$$C_D a = C_{D_{\chi,F}} \left(\frac{U_1}{U_{\chi,F}} \right)^{\chi_F} a_L + C_{D_{\chi,S}} \left(\frac{U_1}{U_{\chi,S}} \right)^{\chi_S} a_S \qquad (7)$$

where $C_{D_{\chi,F}}$ and $C_{D_{\chi,S}}$ are drag coefficients for the foliage (F) and the stem (S), respectively, changing accordingly to the reconfiguration (χ) (-), $U_{\chi,F}$ and $U_{\chi,S}$ are the reference velocity for foliage and stem used to calculate the reconfiguration parameter for the foliage (χ_F) and the stem (χ_S) respectively (m/s), a_L is the frontal area of leaves per unit of water volume (m^{-1}) and a_S is the frontal area of the stem per unit of water volume (m^{-1}). $C_D ah$ can be determined through *Equation 7*, replacing a_L with $A_L/(A_B z)$ and a_S with $A_S/(A_B z)$ where A_B is the bed area (m) and z is the vertical thickness of the considered layer (m), and integrating z over the entire height of the vegetation. $C_D ah$ is used in submerged vegetation approaches and in the definition of density limits according to Nepf (2012a): $C_D ah \ll 0.1$ identifies very sparse vegetation, $0.1 < C_D ah < \sim 0.23$ represents transitional density of plants and $C_D ah > \sim 0.23$ is used to define a dense vegetation. The vegetative friction factor is used, considering the individual plant scale, in 2D depth-averaged models, while, n_{veg} is commonly determined at the reach scale in practical applications.

2.2.2 Theoretical developments in description of flow-vegetation interaction: Momentum equation

The interaction between flow and aquatic plants was studied through the promising *double-averaging methodology* (DAM) that considers average hydraulic variables in time and space (e.g. Nikora et al., 2007a;b). DAM made possible to apply a spatial average to *Reynolds time-Averaged Navier-Stokes equations* (RANS), in situations where ordinary RANS solutions cannot be practicable due to the high complexity of the roughness (Nikora et al., 2007a; Luhar et al., 2008). When the water flow enters in a vegetated patch, it is three-dimensional and spatially heterogeneous in its time-average, because it is forced to change directions many times, following the configuration of vegetation and bed roughness. In these terms, the streamwise momentum equation and the continuity equation, using index notation and common decomposition of variables[9], becomes (Luhar et al., 2008; Nikora et al., 2001; White & Nepf, 2007):

$$\rho\left[\varphi\frac{\partial\langle\overline{u_i}\rangle}{\partial t}+\frac{\partial\varphi\langle\overline{u_j}\rangle\langle\overline{u_i}\rangle}{\partial x_j}\right]=-\frac{\partial\varphi\langle\bar{p}\rangle}{\partial x_i}+\mu\frac{\partial^2\varphi\langle\overline{u_i}\rangle}{\partial x_j^2}+\frac{\partial\varphi\langle\tau_{ij}\rangle}{\partial x_j}+\rho\varphi g-D_i \qquad (8a)$$

$$\frac{\partial\varphi\langle\overline{u_i}\rangle}{\partial x_i}=0 \qquad (8b)$$

where u_i and u_j are velocity components depending on the index i or j (=1,2,3) (m/s), x_i and x_j are the axis with i or j (=1,2,3) (m), p is the pressure (N/m^2) and μ is the water dynamic viscosity (Ns/m^2). τ_{ij} in *Equation 8a* is the shear stress tensor (N/m^2) depending on the turbulent stress and the dispersive stress associated to spatial fluctuations. The formulation of τ_{ij} is:

$$\langle\tau_{ij}\rangle=-\rho\langle\overline{u_i'u_j'}\rangle-\rho\langle\bar{u}_i''\bar{u}_j''\rangle \qquad (8c)$$

In the velocity field in the vertical direction, dispersive stress is countable in vegetation characterized by sparse density ($C_Dah\ll 0.1$) and it is in the same direction as the turbulent stress, close to the bottom of the canopy, and in the opposite direction, near the top (Poggi et al., 2004). In dense canopy, dispersive fluxes can be negligible because they are observed to be less than 10% of the turbulent stress, as resulted from experiments performed by Poggi et al. (2004) with rigid cylinders. D_i in *Equation 8a* is the spatially averaged resistance associated to the canopy elements. It is obtained by the sum of the form and viscous drag:

$$D_i=\langle\frac{\partial\bar{p}''}{\partial x_i}\rangle-\langle\mu\frac{\partial^2\bar{u}_i''}{\partial x_j^2}\rangle \qquad (8d)$$

[9] Decomposition of variables includes, firstly, a time average (overbar) and deviations from it (single prime); then, the time-averaged quantities are divided in spatial mean (angle bracket) and deviations from it (double prime) (Nepf, 2012a).

Within the canopy, the viscous stress is negligible in comparison with the canopy drag (Luhar et al., 2008). For finite Reynolds number, D_i can be derived through different approaches listed by White & Nepf (2007), mostly using a quadratic resistance law.

In order to simplify three-dimensional *Equation 8a-8b* to two dimensions, quantities can be spatially averaged over depth (White & Nepf, 2007). In addition, assuming a long-time average for removing all the temporal fluctuations, the drag becomes a discontinuous function in a partly vegetated channel (White & Nepf, 2008):

$$\langle \overline{D_x} \rangle = \begin{cases} \frac{1}{2}\rho\left(C_D a + \frac{c_f}{h}\right)\langle \overline{U} \rangle^2, & \text{vegetated area} \\ \frac{1}{2}\rho\left(\frac{c_f}{h}\right)\langle \overline{U} \rangle^2, & \text{unvegetated area} \end{cases} \quad (9)$$

where c_f is the bed friction coefficient (-) and $\langle \overline{U} \rangle$ is the spatially depth and time-averaged velocity (m/s). Within the vegetation, the second term in the parenthesis (*Equation 9*) defining the bed friction is much lower than the drag due to the canopy presence and, therefore, it can be neglected (see *Equation 5*). Note that *Equation 8a-8b* include the spatial variation of the vegetation porosity. If the vegetation porosity is less than the unit, *Equation 9* has to be divided by $\varphi = (1 - \phi)$, as Nepf (2012a) suggested. This division reflects the fact that the drag acts only in the volume occupied by the vegetation.

In the attempts to describe the flow field, the problem of the turbulence closure has to be solved. Different studies (e.g. White & Nepf, 2008; Lopez & Garcia, 1998; Defina & Bixio, 2005) focalized their attention on the parametrization of the shear stress distribution using the turbulent kinetic energy and dissipation rate model (*κ-ε model*). The main formulation, commonly used for solving the turbulence closure, includes the terms of the eddy viscosity and mixing length (Siniscalchi et al., 2012; Ma, 2014; Lopez & Garcia, 1998). In partly vegetated channel, coherent turbulent structures are strongest at the vegetation interface, as obtained by White and Nepf (2008). In this area, the trend of eddy viscosity and the one of the mixing length have a peak, decreasing sharply within the vegetation and slightly in the open channel. Note that positive values of the eddy viscosity define the region where energy flux is exchanged from the mean flow to the turbulence.

2.2.3 Flow field at the patch scale

Compared with unvegetated open-channels, where flow patterns are quite symmetric around the centre line, the presence of vegetated patches adds a new effect due to transversal shear, making the two-dimensional schematization of flow useless. The velocity pattern is altered and becomes more inhomogeneous and less symmetric, fluctuating transversally and vertically (Sukhodolov & Sukhodolova, 2010). The flow patterns, at the patch scale of a partly vegetated channel characterized by emergent/submerged plants, are generated by different mechanisms and they can be visualized in the vertical and horizontal sections shown in *Figure 2.4*. As Nikora et al.

(2012) suggested, flow patterns in the vertical plane can be: associated with flow separation from stems (*#1*), attached to leaf/stem surfaces within local boundary layers (*#2*), behind plant leaves (*#3*) and generated by plant waviness at a range of scales (*#4*). In the horizontal plane the turbulence is associated to wakes and flow separation behind the vegetated patches (*#5*) and to the boundary or mixing layer at the patch sides (*#6*).

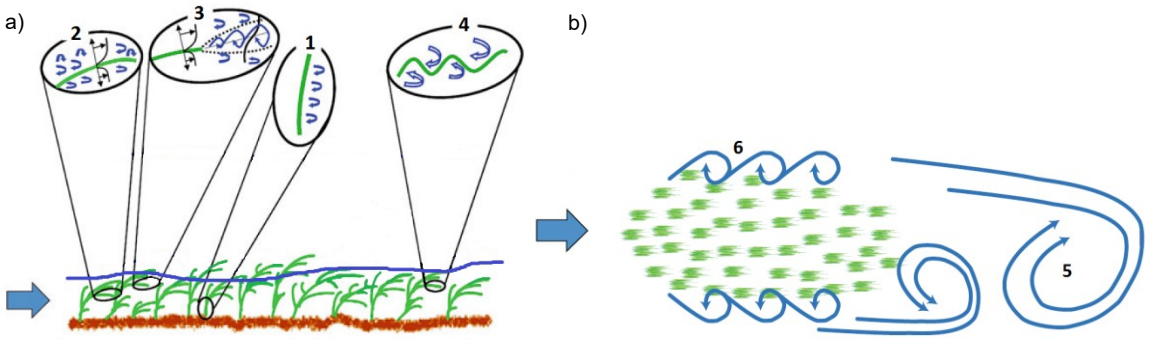

Figure 2.4: Scheme of flow patterns (from *#1* to *#6*) in partially vegetated channel at the patch scale: a) side view, b) top view. (Modified from Nikora et al. 2012)

When the flow encounters a patch, it experiences the stronger roughness of the vegetation in comparison with the bare bed (see *Section 2.2.1*), deflecting in the direction of the unvegetated area. As noticed by Nepf (2012a), this deflection develops within the canopy for a certain length ($x_D \sim 2b$) (see *Figure 2.5*) and it starts upstream in front of the patch at a distance depending on the vegetation density. If the vegetation is dense the longitudinal velocity component starts decreasing and the transversal component increasing further away from the leading edge (Zong & Nepf, 2010). In the *diverging flow region* (see *Figure 2.5*), even if the mean velocity decreases, the turbulence is enhanced likely due to vortices generated at the stem scale, as observed by Nepf (1999) in her experiments with a stem Reynolds number greater than 100. After this zone, Kelvin-Helmoltz (KH) vortices[10], caused by an unstable inflection points at the vegetation interface, start increasing streamwise. This transverse instability dominates the mass momentum exchange between the vegetation and the adjacent open flow. A shear mixing layer[11], similar to the one generated above submerged vegetation, is observed (e.g. Carollo et al., 2002; Luhar et al., 2008; Nepf et al., 2013). If the vegetated patch is long enough, KH vortices start stabilizing and they stop growing in the *fully developed flow region* (see *Figure 2.5*). In this region, the cross-section velocity profile can be determined using two-dimensional models, as different research activities verified (e.g. White & Nepf, 2008; Zong & Nepf, 2010; Nepf, 2012a). If the patch of emergent plants is located far away from the riverside, two flow-parallel edges, symmetric to the x axis in *Figure 2.5*, are generated. According to Nepf (2012b) and Rominger & Nepf (2011), these edges cause surface displacements that are shifted of half-cycle phase. When at one edge there is a minimum in pressure, in the other side the pressure has a maximum.

[10] Instability generated by the presence of velocity shear in a continuous fluid.
[11] Zone of the flow between two regions of constant velocity, containing an inflection point in the velocity profile, enhanced correlation between velocity fluctuations and structure of momentum transfer (Ghisalberti & Nepf, 2002).

According to White & Nepf (2008), in the shear mixing layer the same volume of water is transported from unvegetated area to the canopy patch (*sweeps*) and from the patch to the open channel (*ejections*) during a realization of a vortex within a certain period and wavelength, imposing the mass conservation. As they noticed, these two phenomena are strictly linked to the lateral Reynolds stress ($\sim\langle\overline{u'v'}\rangle$): sweeps are generated when the longitudinal velocity time-fluctuation (u') is positive and the transverse velocity time-deviation (v') is negative; while, ejections are caused when u' is negative and v' is positive. The correlation of velocity fluctuations is appreciable just close to the centre of vortices. Further away, the lateral Reynolds stress becomes almost null ($\langle\overline{u'v'}\rangle \approx 0$) due to the enhanced variation of fluctuations across zero. In comparison with the free shear layer, where flow vortices continue to grow and merge, in the partly obstructed shear flow the width of vortices reaches an equilibrium. This equilibrium is due to the production of kinetic energy from sweep events in the outer layer that balances its dissipation due to the presence of the vegetation interface (White & Nepf, 2007).

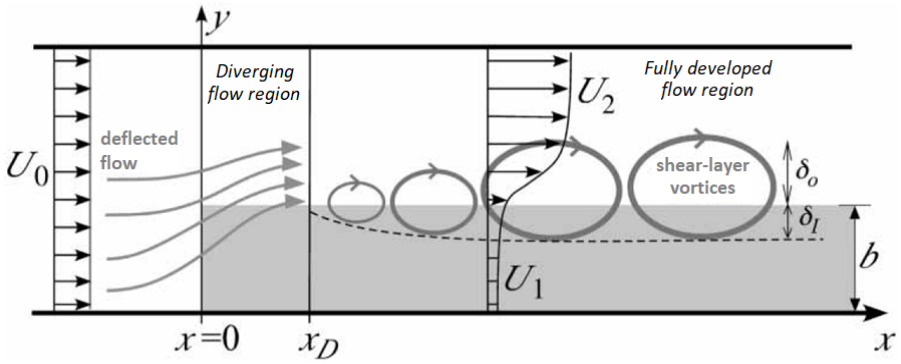

Figure 2.5: Top view of a channel partly vegetated with the identification of different flow regions. The pattern fill represents a patch of emergent canopy (Modified from Nepf 2012b).

In the fully developed flow region, the shear layer is asymmetric to the vegetation interface: the streamwise velocity varies sharply into the vegetation and more gradually in the open channel. Two different penetration lengths of turbulent stresses can be detected for the inner (δ_I) and the outer layer (δ_O), as shown in *Figure 2.5*. According to White and Nepf (2007), within the thickness of the inner layer, the interfacial shear stress balances the canopy resistance. In the outer layer, the shear stress balances the pressure gradient from the free surface slope and the turbulence term does not cause substantial momentum flux. The length scales of δ_I and δ_O can be approximated as (White & Nepf, 2007):

$$\delta_I \sim max((C_D a)^{-1}; d) \qquad (10a)$$

$$\delta_0 \sim {}^{h}/_{c_f} \qquad (10b)$$

For sparse vegetation ($C_D ah \ll 0.1$), δ_I and δ_O tend to be quite similar; while, for dense canopy ($C_D ah > \sim 0.23$), δ_O becomes much higher than δ_I and the ratio ${}^{\delta_I}/_{\delta_O}$ tends to be null (White & Nepf, 2008). The assumption of a symmetric penetration of the shear mixing layer beside of the vegetation interface resulted in an overprediction of the penetration

length of the turbulence within the dense vegetation, as observed by van Prooijen et al. (2005).

2.3 Transport of fine sediments and vegetation interaction

The transport of particles in unvegetated channels was widely studied using several models, based on the mean bed shear stress (e.g. van Rijn, 1984; James et al., 2002) or on the role of turbulence (e.g. Celik et al., 2010). Within vegetated patch, more complex processes have to be taken into account and ranges of applicability for known equations may be not complied. For example, the bed shear stress varies within the vegetation and the turbulence is mostly due to vegetation drag (F_D), as Vargas-Luna et al. (2015) and Västilä (2015) suggested. The bed shear stress decreases passing from bare bed to vegetated bed and it varies spatially at the stem scale (e.g. Nepf, 2012b). Often, variables that characterize transport of sediments in canopy patch are defined as those along the open channel plus new variable characterizing the vegetation (Lopez & Garcia, 1998; Västilä et al., 2016).

In rivers or channels, vegetated patches are not stable, but they change continuously in shape and size, interacting with suspended sediments. Chen et al. (2012) and Nepf (2012a) studied the movement and the reallocation of fine sediments along the longitudinal direction of a vegetated channel. Sediments enter in the emergent vegetated patch because they are transported by advection through the leading edge (e.g. Zong & Nepf, 2010; 2011) and by turbulent diffusion at the vegetation interface parallel to flow direction (e.g. Sharpe & James, 2006). The deposition is enhanced behind the patch, when the turbulent kinetic energy is low enough (Ortiz et al., 2013). The large-scale turbulent kinetic energy is converted to small-scale turbulent kinetic energy within the vegetation, reducing the turbulent diffusivity and increasing the net deposition (Nepf, 1999). Field and laboratory experiments of Zong & Nepf (2010), Sharpe & James (2006) and Västilä & Järvelä (2017) revealed that the net deposition is strongly dependent on flow conditions, characteristics of sediment and location of the feeding point. According to Elliott (2000), the settling is enhanced by vertical mixing within the vegetation compared to the net deposition in the open channel. Abt et al. (1994) estimated that the presence of the vegetation can increase the entrapment of sediment by 30-70%. This percentage varies according to the height of the plants: in emergent vegetation it is higher than in submerged vegetation. In partly vegetated channel, the vegetation retained about 80% of sediments entering the patch and this value depends on the vegetation density, as Zong & Nepf (2010) suggested.

2.3.1 Sediment properties

The suspended concentration and the net deposition distributions along the partly vegetated channel are influenced by the grain size of sediment used in the experiments. The fraction of fine sediment is transported in suspension, while larger particles mostly tend to move close to the bed as bed load and can settle. Abt et al. (1994) and Sharpe & James (2006) observed that sediment distribution showed less large particles and more fine-medium fractions of grain size in the deposition the further they moved away from the feeding point for measurements. A common classification of sediment divides cohesive particles, when about 10% of the finer fraction has a characteristic diameter lower than 0.063 mm, to non-cohesive ones, characterized by a higher characteristic diameter. This distinction plays an important role for defining different behaviours in transport processes. According to Sun et al. (2018) and McAnally & Mehta (2002), the inter-particle cohesive force influences the structural density, deflects trajectories of suspended sediment due to the form and disaggregation of flocs[12] and requires higher critical shear stress to initiate the motion.

The particle settling velocity influences the sediment transport processes and it can be estimated from laboratory experiments or predicted using empirical formulae (e.g. Jimenez et al., 2003). The common simplification of particles into spheres used for artificial sediment does not apply to natural sediment. Formulations have to consider a shape factor for avoiding large errors in the estimation of the settling velocity (e.g. van Rijn, 1984; Graf, 1971; Dietrich, 1982). Moreover, the settling process depends on the concentration and properties of sediments: when the concentration is very low, particles do not interact among each other, when the concentration is high, the settling can be hindered or enhanced because particles are forced to settle all together (van Rijn, 1984). On one hand, when sediments tend to aggregate in flocs, they can form larger particles settling faster. On the other hand, flat large particles can be floating and never settle.

2.3.2 Transport processes in partially vegetated flow

The transport of sediment is defined as the entire solid transport passing through a cross-section of a river or channel (Graf, 1998). In vegetated flow, Nepf (2012a) suggested the application of the *double-averaging method*[13], assuming that there are no sources or sinks and using index notation and common decomposition of variables (see *Section 2.2.2*):

$$\frac{\partial\langle\bar{C}\rangle}{\partial t} + \langle\bar{u}_j\rangle\frac{\partial\langle\bar{C}\rangle}{\partial x_j} = -\frac{1}{(1-\phi)}\frac{\partial}{\partial x_j}(1-\phi)\left\{\langle\overline{u_j'C'}\rangle + \langle\bar{u}_j''\bar{C}''\rangle - D_m\langle\frac{\overline{\partial C}}{\partial x_j}\rangle\right\} \qquad (11)$$

where C is the sediment concentration (kg/l) and D_m is the molecular diffusion (m^2/s). In the right-hand side of *Equation 11*, the first term represents the dispersion associated with

[12] Very fluffy mass generated by the aggregation of fine suspended particles.
[13] Method that takes into account the averages in time and space of all the variables.

turbulence fluctuations (i.e. turbulent diffusion), the second term is, according to Nepf (1999), caused by spatial heterogeneity in the time-mean velocity field (i.e. tortuosity), the third term is due to the molecular diffusion. As Zong & Nepf (2010) observed, the turbulent diffusion and the mechanical dispersion play the main role in the transport of fine sediment and the molecular diffusion can be neglected.

In vegetated patches characterized by cylinder shape-like woody vegetation (*Figure 2.6*), Tanino & Nepf (2008), Vargas-Luna et al. (2015), Västilä & Järvelä (2017) and Luhar et al. (2008) affirmed that transport of fine sediment varies according to vegetation density. When vegetation is dense ($C_D ah > \sim 0.23$ in *Figure 2.6*), the contribution of the turbulent diffusion declines rapidly because the momentum transferred by shear-layer vortices is dissipated by the high vegetation drag, enhancing deposition and settling. The mechanical dispersion due to the spatial variability becomes more important. For sparse canopy ($C_D ah \ll 0.1$ in *Figure 2.6*), the turbulent diffusion is the main process inducing transport close to the bed. The erosion and the resuspension are the main effects.

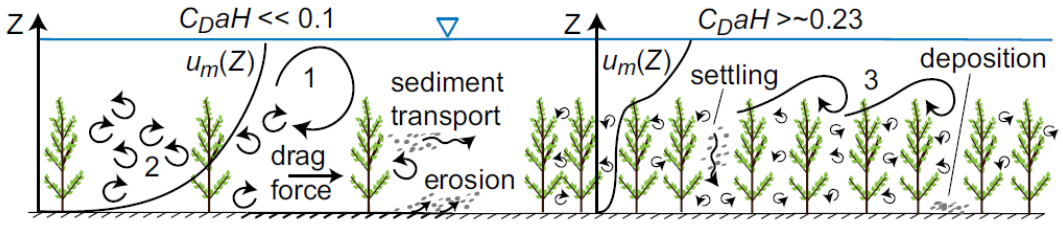

Figure 2.6: Dominant sediment processes within sparse plant stands ($C_D ah \ll 0.1$) and dense plant stands ($C_D ah > \sim 0.23$). The pattern *#1* relates to the turbulence generated by depth-scale shear, *#2* individual plants and *#3* stand-scale shear layer (Västilä, 2015).

The net deposition of suspended particles exists when the bed shear stress is lower than a certain critical value related to sediment properties (Västilä, 2015). The rate of deposition can be determined by imposing the boundary condition, described by *Equation 12*, to the conventional diffusion-convection transport process (Sharpe & James, 2006):

$$\varepsilon_z \frac{\partial C}{\partial z} + (1 - P) w_s C = 0 \qquad (12)$$

where ε_z is the sediment diffusivity in the vertical direction z (m^2/s), P is the probability that a particle reaching the bed will not be re-suspended again (-) and w_s is the particle settling velocity (m/s). If a parabolic vertical profile for ε_z is considered, at the free water surface ε_z is null. Consequently, the concentration of suspended particles is also null, according to *Equation 12*.

In partly vegetated channel, phenomena related to processes of transport are more complex due to lateral interaction between the open channel and the vegetation interface. The suspended sediment concentration within the vegetation is lower compared to the one observed in the open-channel, consequently to the reduction of the averaged streamwise velocity. The net deposition is not always related to mean flow velocity and mean bed shear stress, but it depends on the turbulent level (e.g. Ortiz et al., 2013). In the diverging flow region, fine sediments settle in the open-cannel due to the high lateral mass transfer

generated by the deflected flow from the vegetation to the unvegetated area, as Zong & Nepf (2010) observed. In the fully developed flow region, the transverse diffusivity (ε_y), at the vegetation interface, is enhanced about one order of magnitude compared to ε_y outside the inner layer (δ_I) (Sharpe & James, 2006). This enhancement is due to the presence of coherent vortices (see *Section 2.2.3*). As noticed by White & Nepf (2007), vortices in the shear mixing layer have two different rotations: inward close to the bed and outward at the free surface. This difference is due to the unbalance equilibrium between the radial pressure gradient and the tangential acceleration in the bottom boundary layer and it contributes to generate a vertical mass transfer at the vegetation interface other than the transversal one (White & Nepf, 2007). Within δ_O, the turbulent diffusivity (ε_i) is strictly connected to the variation of streamwise velocity and thickness of the shear layer. Within the vegetated patch, in δ_I, ε_i is influenced by the vegetation and its geometry (see *Section 2.1.1*), while outside δ_I, where the streamwise velocity is uniform, ε_i is generated at the stem-scale (Zong & Nepf, 2010).

Västilä & Järvelä (2017) tested some factors such as the cross-sectional vegetative blockage factor, the flow velocity within the vegetation and the distance from the feeding point, using a multiple regression analysis and net deposition on field measurements in a partly vegetated channel. Their results affirmed that the cross-sectional vegetative blockage factor, depending on the height of the vegetation, had a direct influence on the net deposition. While, the flow velocity within the vegetation and the distance from the feeding point had a reverse influence. Sharpe & James (2006) observed a longitudinal deposition profile characterized by a decreasing exponential curve, going downstream from the feeding point.

2.4 Research gap

Although, in the hydraulic prospective, effects of the vegetation in the water flow were studied in the past, just in the recent 20 years, the interaction between flow and vegetation was considered in its interdisciplinary complexity (i.e. physical, chemical and biological aspects). Due to differences in properties among plant species, flow patterns and transition zones, generated by interactions in multi-scale boundary layers, can be still unknown (e.g. Nikora, 2010; Nikora et al., 2012; Nepf, 2012b). As Folkard (2011) noticed, research activities have been lacking of agreement in conventions and use of variables, due to the different purpose/scale and different approaches used (e.g. field campaigns, laboratory experiments with natural, artificial plants, rigid or flexible elements). These differences affect the reliability of results and predictions for the management of channel and control of water quality. Estimation of variables, used to describe plant morphology and density, are challenging to obtain for natural vegetation (e.g. Vargas-Luna et al., 2015). The variation in properties is also due to the season and hydraulic conditions, as suggested by Nepf (2012b) and Siniscalchi et al. (2012).

Transport of sediments has been widely studied in unvegetated channels and recent focus has been on the interaction with riverine vegetation. The models applied in the past studies cannot be totally reliable for vegetated channels, because the turbulence is caused mostly by the vegetative drag instead of the bed shear stress (Västilä & Järvelä, 2017). Aquatic plants interact on suspended sediment load and deposition. Formulations, describing transport processes and incorporating properties and effects of vegetation, are still lacking (Vargas-Luna et al., 2015). In partly vegetated channels, the characterization of suspended sediment concentration within and across vegetated patches was mostly described over time. Data of higher spatial resolution is needed for the physical understanding of suspended sediment processes, as noticed by Västilä (2015). Also, long-term effect of vegetation in river morphology such as evolution of vegetated patches and changes in vegetated characteristics during their life cycle, should get more attention (Vargas-Luna et al., 2015).

3. Materials and methods

A brief overview on measurement approach and methodology is shown in *Figure 3.1*. Experiments were performed in a partly vegetated flume with emergent natural-like flexible plants under steady uniform flow conditions. Two vegetative conditions were investigated: foliated vegetation representing spring/summer period and leafless vegetation representing autumn/winter period. Measurements, experimental setting and data analyses are described in detail in the following sections of this chapter.

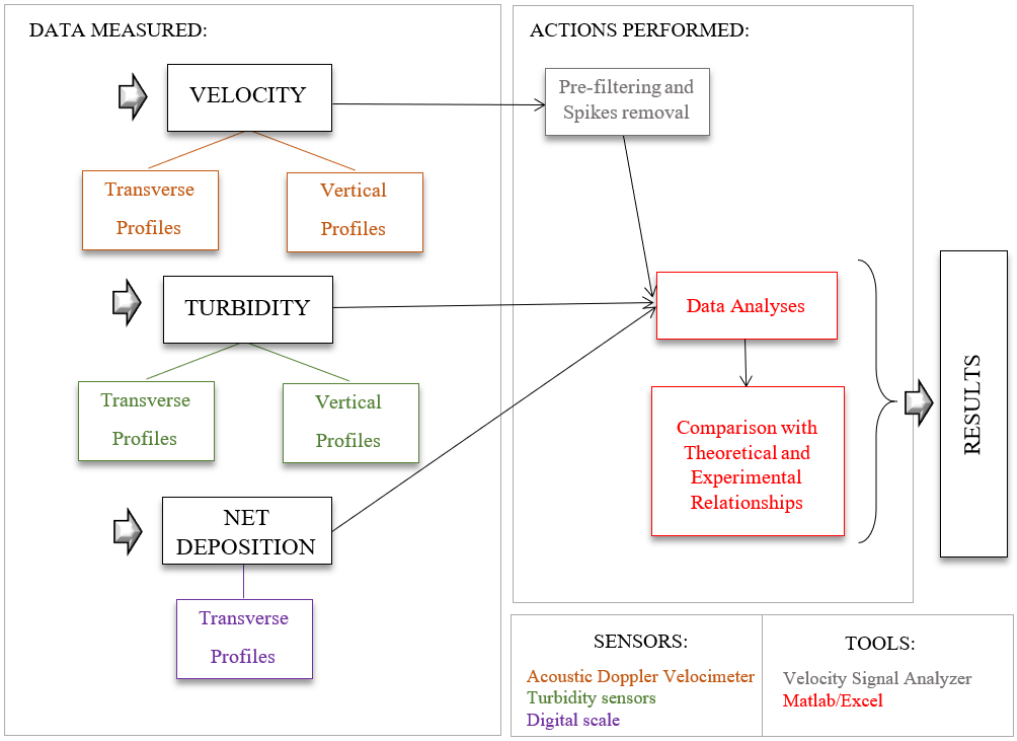

Figure 3.1: Visual scheme describing data measured and action performed (e.g. data treatment, analyses and fitting with theoretical and experimental equations) for the two vegetative conditions: foliated and leafless. Different colours underline which kind of sensor for measurements or which kind of tool for analyses was used.

3.1 Experiments in the hydraulic flume

Experiments on the characterization of the velocity field and transport processes in the partially vegetated channel (*Figure 3.2-3.3*) were conducted in a hydraulic flume. *Table 3.1* shows the main dimensions and tilting range of the hydraulic flume used. The working section length (see *Table 3.1*) was lower than the total length of the flume for minimizing the effects due to the entrance and the exit of the water flow. In the beginning of the flume there was a damping device to ensure the smooth entrance of the flow, while in the end of the flume there was a weir. The mode A for the recirculation of the water was used: discharge up to 0.120 m^3/s, complete stand-alone, self-contained circulation system with the possibility to vary the speed of pumps through magnetic flow meter and adjust the

flow. The steady uniform flow was established by adjusting the weir located in the end of the flume and the bottom slope.

Table 3.1: Main dimensions of the hydraulic flume.

Variable	Value
Total length (m)	20.3
Working section length (m)	16.0
Width (m)	0.60
Depth (m)	0.80
Tilting range (%)	-0.75 to +2.1

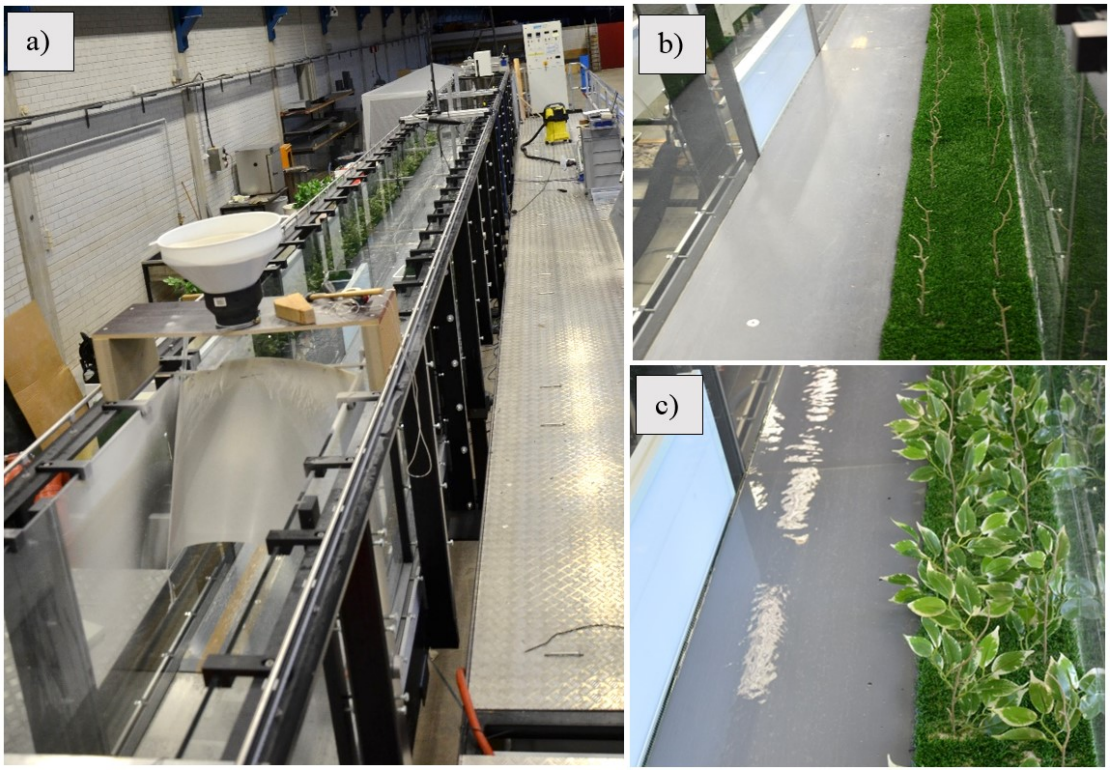

Figure 3.2: Pictures taken in the Environmental Hydraulics Lab in Aalto University showing: a) hydraulic flume used for the experiments with the feeding system in the foreground, b) working section of the partly vegetated flume in the leafless condition, c) working section of the partly vegetated flume in the foliated condition.

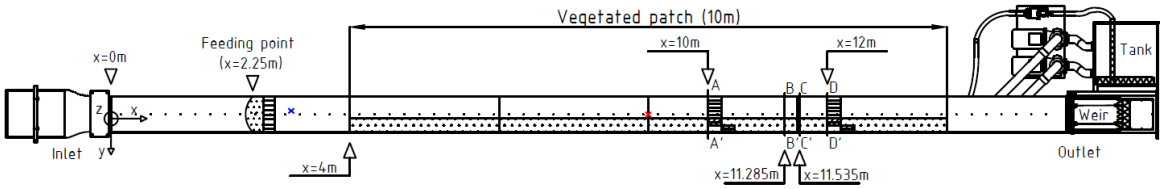

Figure 3.3: Top view of schematic overview of the partly vegetated hydraulic flume used in the experiments with the main dimensions and the coordinate system. In cross-sections A-A', D-D' net deposition measurements were performed. In cross-section B-B', C-C' velocity and SSC measurements were carried out. The blue cross represents the location in which the Vectrino+ probes were oriented. The red cross represents the location where the reference SSC measurements were collected.

The partly vegetated flume was characterized by a 10 m long and 0.23 m wide vegetated patch. The patch was positioned along one side of the flume (see *Figure 3.3*) and it

included understory grass mat of 2 cm thickness and emergent/submerged flexible natural-like plants. The plants were placed in a staggered pattern, repeated every 0.5 m, as shown in *Figure 3.4*. In the foliated condition, the vertical distribution of the leaves was tested prior to this work to optimize the uniformity of the velocity profile within the vegetated patch.

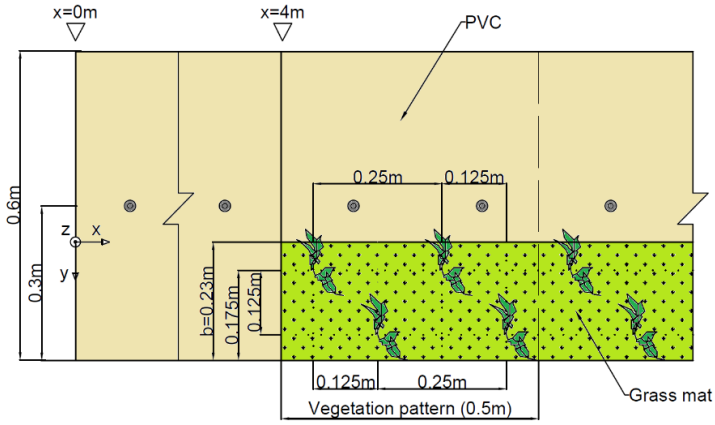

Figure 3.4: Main dimensions of the bed of the partly vegetated flume and the vegetated pattern used in the experiments.

To investigate the seasonal changes, morphological properties of the artificial plants were defined, taking into account stems and leaves (see *Section 2.1.1*). *Table 3.2* lists the frontal project areas per unit bed area (A_f/A_B) and the bulk frontal areas per unit water volume (a), considering leaves (A_L/A_B and a_L) and stems (A_S/A_B and a_S), respectively. For the foliated vegetation the frontal project area of the leaves (A_L) was calculated from the leaf area index (see *Section 2.1.1*) representing one-sided leaf area per unit bed area.

Table 3.2: Frontal project areas per unit bed area (A_L/A_B, A_S/A_B) and bulk frontal areas per unit water volume (a_L, a_S) for leaves and stem. The letters L, B and S identify leaves, bed and stem, respectively.

Variable	Value
A_L/A_B (m^2/m^2)	0.7
A_S/A_B (m^2/m^2)	0.02
a_L (m^{-1})	4
a_S (m^{-1})	0.11

Table 3.3 shows the hydraulic flow conditions and the corresponding bed slope for both vegetative conditions. The patch was long enough to allow the generation of the fully developed flow region, in which measurements were carried out. The sediment feeding point (see *Figure 3.3*) was located at 1.75 m in front of the leading edge of the vegetation. This distance upstream the vegetated patch allowed a complete mixing of the suspended sediment along the flume section. The sediment feeding rate was 2.8 g/s, constant for the entire sampling time. The water level was constantly monitored, using six pressure sensors integrated in the bottom of the flume.

Table 3.3: Experimental hydraulic conditions for leafless and foliated condition. Q is the discharge, S is the bottom slope, and h is the water level.

Vegetative condition	Q (m^3/h)	S (%)	h (m)
Leafless	180	0.17	0.1715
Foliated	180	0.37	0.171

3.1.1 Sensors and instrumentations

Instantaneous 3D velocity measurements were performed using a down-looking and side-looking Vectrino+ 3D Acoustic Doppler Velocimeter (ADV) probe, manufactured by Nortek (see *Figure 3.5*). Transverse profiles were measured using the side-looking probe (i.e. right-looking probe). For vertical profiles, it was not possible to use only the down-looking probe due to the distance between the probe and the sampling volume. The down-looking probe was used for measurements closer to the bed and the side-looking probe for measurements closer to the free water surface. The functional principle of these devices was the *Doppler Effect*[14]: the central transducer transmitted short pairs of sound pulses whose echoes were listened by four beans placed around the transducer. Velocity measurements were obtained by measuring the change in pitch or frequency of the returned sound, reflected by particles suspended in the water flow. The sampling volume (see *Table 3.4*) had a cylinder shape and a height that could be set by the user. The resolution of Vectrino+ ADV probe was ± 0.3 mm/s.

Table 3.4: Sampling volume characteristics for Vectrino+ ADV probe (Nortek AS, 2009).

Variable	Value
Distance from the probe (mm)	50
Diameter (mm)	6
Height (mm)	3-15

[14] Effect due to a change in pitch heard when the source of the sound or the listener is in motion. For example, it is the same effect generated when a siren on a vehicle is moving closer or further to or from the listener.

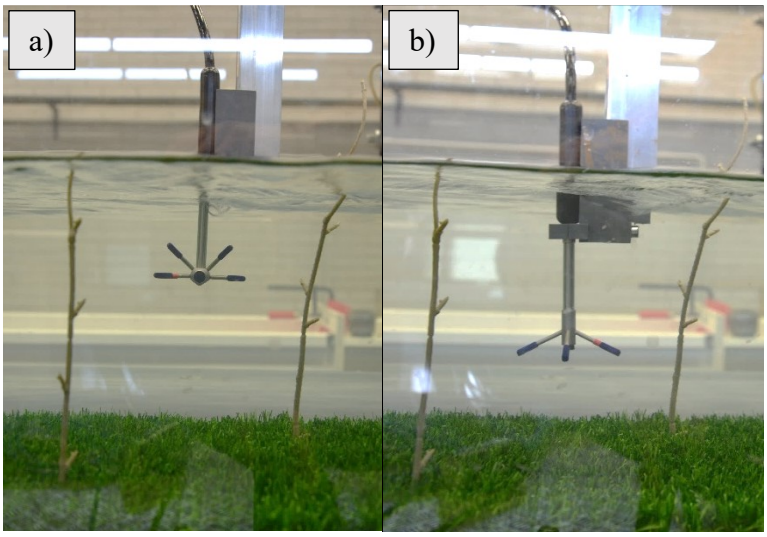

Figure 3.5: Vectrino+ ADV sensors used to measure 3D instantaneous velocity: a) side-looking probe, b) down-looking probe.

Turbidity measurements were performed with four sensors: two nearly identical OBS-3+ and two nearly identical NEP5000 sensors (see *Figure 3.6*). The functional principle was the same for both: a near infrared (NIR) laser and photodiode detected the intensity of the light scattered by suspended particles moving in the water flow. The data logger powered the device and digitized the analog signals. The conversion in Suspended Solids Concentration (SSC) values can be performed in post-processing, if the linear calibration curve that links NTU[15] values to SSC is known. The sampling volume had a cone shape and it could vary in size depending on the turbidity detected (see *Table 3.5* for OBS-3+ sensors). The sensor NEP5000 had a smaller sampling volume and it localized better the measurements of scattering. It had, also, an automatic real-time cleaning system for the probe. NEP5000 sensors were extremely accurate and stable at very low NTU values, allowing high resolution reading close to zero NTU (Observation Instruments, 2015). The accuracy of the OBS-3+ sensor was, for sand sediment, ± 4% of the reading or ± 10 mg/l. The accuracy of the NEP5000 sensor was ± 1%. Due to the difference in accuracy, transverse SSC profiles were measured using NEP5000 sensors in the foliated condition. OBS-3+ sensors were used for measurements of transverse profiles in leafless condition and for vertical profiles.

Table 3.5: Sampling volume characteristics for OBS+3 sensor (CSI, 2008).

Variable	Value
Max height from the probe in very clear water (mm)	500
Angle at the top of the cone (º)	42
Volume (mm^3)	$25\text{-}12*10^4$

[15] Nephelometric Turbidity Units.

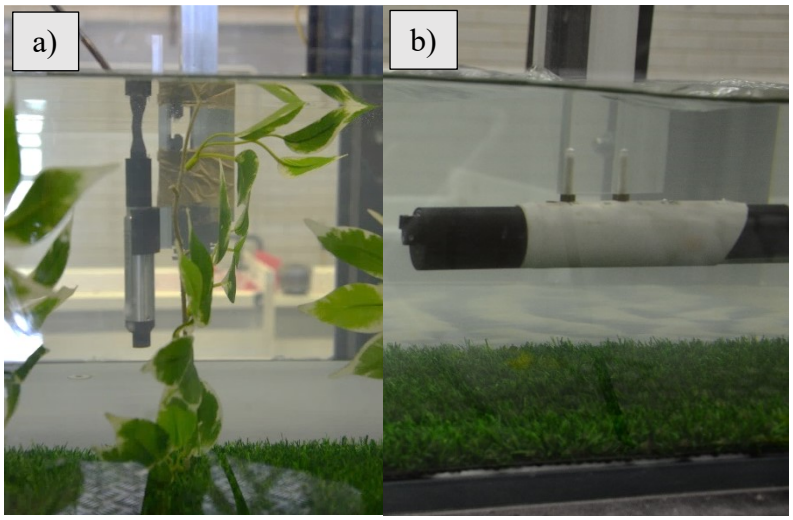

Figure 3.6: Turbidity sensors used to measure SSC: a) OBS-3+ sensor, b) NEP5000 sensor.

3.1.2 Fine sediment characteristics

Natural sediment used in the experiments was produced by Sibelco Benelux and classified as fine sand *S90*. The chemical composition was: 99.5 % of SiO_2, 0.2 % of Al_2O_3 and Fe_2O_3 and TiO_2 in traces. The physical properties were: particle density (ρ_p) of 2.65 kg/dm^3 and hardness of 7 in Mohs scale. The granulometric curve was quite narrow, as shown in *Figure 3.7*.

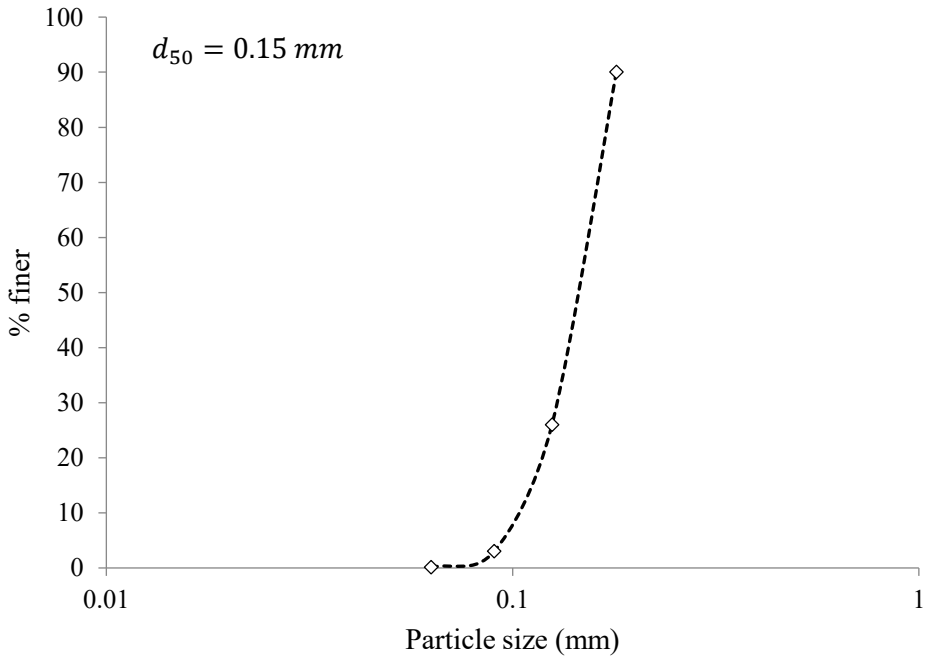

Figure 3.7: Granulometric curve of fine sediments *S90* as reported by the manufacturer (Sibelco Benelux, 2009).

The median diameter (d_{50}), sieve size with 50% of finer sediments passing, was 0.15 mm. To describe grading characteristics, the gradation coefficient (C_C) and the uniformity coefficient (C_U) were calculated (Ishibashi, & Hazarika, 2010):

$$C_C = \frac{d_{30}^2}{d_{60} d_{10}} \quad (13)$$

$$C_U = \frac{d_{60}}{d_{10}} \quad (14)$$

where d_{30} is the size of the sieve with 30% finer sediments passing (m), d_{60} is the size of the sieve with 60% finer sediments passing (m) and d_{10} is the size of the sieve with 10% finer sediments passing (m). In the Unified Soil Classification System (USCS), a soil is considered uniformly graded if C_U is lower than 6 for sands, and well-graded if C_C is between 1 and 3. $S90$ complied all these requirements: C_C was equal to 1.05 (*Equation 13*) and C_U was equal to 1.54 (*Equation 14*). The assumption was that particles were homogeneous and they behaved in the same way when moving in the water flow.

Since the natural sediment had a really low percentage of cohesive particles (< 0.1 %), flocculation processes were commonly not observed and not considered in this study. The settling velocity, taking into account d_{50} as median particle size, was calculated through an iterative procedure: the particle Reynolds number (Re_p) and the drag coefficient (C_D) were iteratively calculated until the difference between their values was below $o(10^{-3})$ size order. The equations used to the determination of Re_p and C_D considered the presence of spherical particles (Turton & Levenspiel, 1986):

$$Re_p = \frac{w_{ss} d_{50}}{v} \quad (15a)$$

$$C_D = \frac{24}{Re_p}\left(1 + 0.173 {Re_p}^{0.657}\right) + \frac{0.413}{1+1.63*10^4 {Re_p}^{-1.09}} \quad (15b)$$

where w_{ss} is the settling velocity of spherical particles (m/s) and v is the kinematic viscosity ($1.003 * 10^{-6}$ m^2/s). The settling velocity of non-spherical particles (w_s) was determined by multiply w_{ss} to a shape factor of solid particles (ξ) (Wilson et al., 2006):

$$w_s = \xi w_{ss} \quad (16)$$

ξ depends on the volumetric shape factor ($K = 0.26$ for sand) and, for sand particles, it can be calculated analytically through an approximation of curves shown in *Figure 3.8* (Grace, 1986):

$$log_{10}\xi = -0.3073 + \frac{0.0656}{cosh(2.55[log_{10} d_* - 1.114])} \quad (17)$$

$$d_* = \sqrt[3]{\frac{\rho(\rho_p - \rho)g}{\mu^2}}\, d_{50} \quad (17b)$$

where ρ is the water density (1000 kg/m^3), g is the acceleration gravity (9.81 m/s^2), μ is the dynamic viscosity of the water ($1.002 * 10^{-3}$ Ns/m^2) and d_* is the dimensionless particle diameter (-).

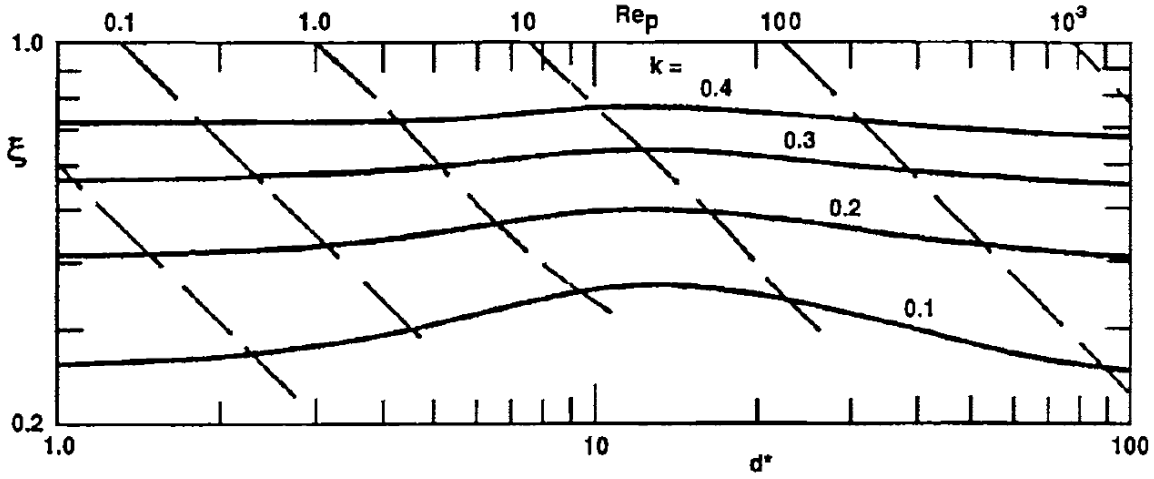

Figure 3.8: Relationship between the shape factor ξ and the dimensionless particle diameter d_* (Grace, 1986).

Table 3.6 summarizes the values of different variables obtained through the calculation of the settling velocity of $S90$ sediment.

Table 3.6: Results of different variables obtained with the iterative procedure used to calculate the settling velocity.

Variable	Value
w_s (m/s)	0.0082
w_{ss} (m/s)	0.0155
ξ (-)	0.53
Re_p (-)	2.324
C_D (-)	13.436

3.1.3 Experimental setup and measurement techniques

3D instantaneous velocity was measured using Acoustic Doppler Velocimeters (ADVs) with a sampling period of 125 s and at a sampling rate of 200 Hz, in two different cross-sections located in the fully developed flow region: cross-section B-B' and cross-section C-C' in *Figure 3.3*. Along the cross-section C-C', three vertical profiles (one in the open–channel, one at the vegetation interface and one within the patch) were measured. For transverse velocity profiles, 21 measurements points were detected, starting 10 cm away from the glass wall in the open-channel, in order to avoid the influence due to the solid boundary. In the unvegetated area, data were measured with an interval of 5 cm, at the vegetation interface at every 1.5 cm and, within the vegetation, with an interval of 3 cm. For the vertical profiles, 9 sampling points were defined every 1.5 cm (skipping the point at 0.07 m), starting 1 cm from the bottom, in the open channel and at the vegetation interface, and 2.5 cm within the vegetation, because of the presence of the grass mat.

SSC measurements were carried out using OBS-3+ sensors with a sampling rate of 10 Hz and NEP5000 sensors with a sampling rate of 5 Hz. The sampling period was of 60 s and the cross-sections were the same used for velocity measurements. Verticals profiles were measured along the cross-section C-C' for five sampling locations: two in the open–channel, one at the vegetation interface and two within the patch. For transverse SSC profiles, 13 measurements were carried out with an interval ranging between 5 and 10 cm in the open channel. At the vegetation interface and within the vegetated patch, the intervals ranged between 1.5 to 3 cm. For vertical profiles, 7 sampling points were measured at intervals of 1.5-3 cm. SSC measurements started at 1 cm from the bottom, in the open channel and at the vegetation interface, and at 2.5 cm within the vegetation, because of the presence of the grass mat. One of the two identical turbidity sensors was always placed at the reference position ($x = 9$ m, $y = 0$ m, $z = 0.095$ m) (see *Figure 3.3*) to detect increase in the concentration of the background resulting from the sediment recirculation and correct the measured data during the pre-processing. The reference point was also used to compare the turbidity detected in different experiments. Due to the difference in the cleaning accuracy and the amount of sediment present in the tanks in the inlet and in the outlet of the flume, the initial concentration of suspended sediment moving in the water flow varied a little bit between different experiments.

Note that when SSC and velocity measurements were clearly influenced by the staggered vegetation, sampling points were shifted 0.125 m downstream in longitudinal direction (*Figure 3.4*).

Measurements of net deposition were performed after 1 h from the start of the feeding in two cross-sections: upstream (cross-section A-A' in *Figure 3.3*) and downstream (cross-section D-D' in *Figure 3.3*) of the velocity and SSC measurements. The flume was slowly drained to avoid sediment movement. Within the vegetation, four strips of grass mat ($5.6x20$ cm^2) were removed carefully and washed in plastic bowls with a known weight. The strips were labelled from A to D, where A was the strip next to the glass wall and D was the one at the vegetation interface. Along the open-channel, other six strips were drawn on the bottom plane and sediments were collected, using a brush, in other small containers characterized by known weight. The collected sediments were dried in an industrial oven, at the temperature of 105ºC, and weighted using a digital scale with a resolution of 0.01 g. The value of net deposition was obtained by the difference between the weight of containers with sediments and the weight of empty containers.

3.2 Data pre-processing

Before starting data analyses, velocity and SSC measurements were pre-processed. ADV measurements were pre-treated through a specific software, following a standard practise used for removal of spikes. SSC data were adjusted removing the background increase. In the next sections, the pre-processing procedures are explained in detail.

3.2.1 Pre-processing of ADV measurements

Measurements of 3D flow velocity have been filtered for removing spikes, using the software Velocity Signal Analyzer[16] (VSA). The method used for filtering was the *Modified Phase-Space Thresholding*, propose by Parsheh et al. (2010). In the original *Phase-Space Thresholding* (PST) technique (Goring & Nikora, 2002), some valid data points next to spikes were incorrectly flagged as spurious data and, consequently, eliminated. The modified phase-space thresholding technique removed, firstly, the obvious spikes characterized by a large magnitude compared to the rest of the data set. Data points with a velocity fluctuation ($u' = u - \bar{u}$) within the range described by *Equation 18* were flagged as valid and unchangeable (Parsheh et al., 2010):

$$-C_1\theta_u \leq u' \leq C_1\theta_u \qquad (18)$$

where C_1 is an arbitrary threshold parameter (-) and θ_u is the median absolute deviation of the velocity time series (m/s). Secondly, spikes characterized by lower magnitude were identified using the PST ellipsoid, comparing the velocity fluctuations (u') with the expected maximum value (u_m) calculated as (Parsheh et al., 2010):

$$u_m = C_2\theta_u\sqrt{2\ln(n)} \qquad (19)$$

where C_2 is an empirical constant (-) and n is the number of data points (-). Every absolute value of data points higher than the expected maximum value was removed. According to Wahl (2003), approximated values for C_1 and C_2 were assumed to be 1.483 and spikes were replaced by the last good value. When C_2 is equal to 1.483, the scale estimator on the median absolute deviation (θ_u) is analogous to the standard deviation (Wahl, 2003).

Velocity data were pre-filtered through the correlation and signal-to-noise ratio (SNR) technique, using the same software as the removal of spikes. The acceptable limits were set as: 70 % for the correlation and 15 for the SNR. The percentage of good data gotten depended on the vegetative condition: for the leafless condition, the percentage of good data was higher than 95% in vertical profiles and 90% in the transversal ones, for the foliated condition, the percentage of good data was higher than 78% in vertical profiles and higher than 75% for transverse profiles. *Figure 3.9* shows an example of velocity data before the removal of spikes and after it, the percentage of good values for this measured point was about 94%.

[16] Software open source for treating and analyzing 3D velocity data from Vectrino+ 3D Acoustic Doppler Velocimeter (ADV) probe. (Jesson, Bridgeman, & Sterling, 2015)

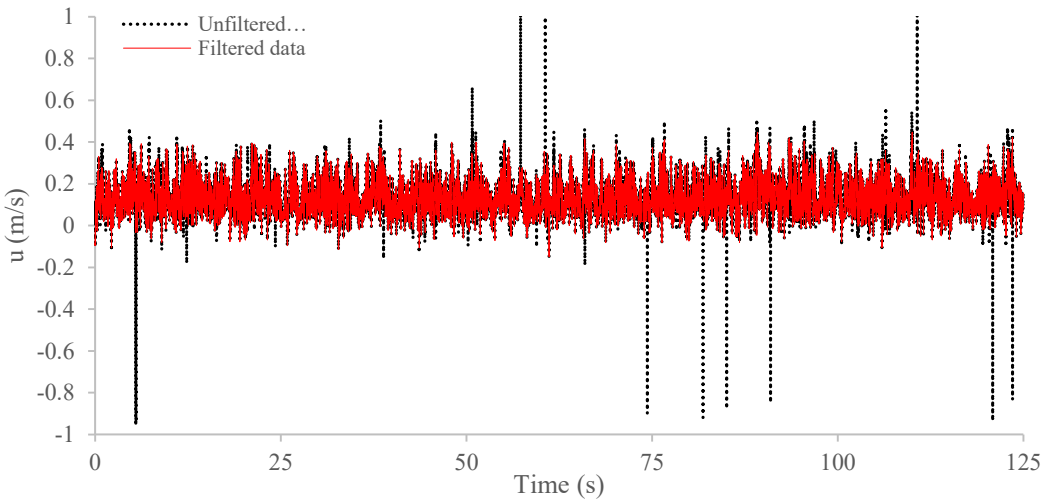

Figure 3.9: Plot of velocity data set before removing of spikes (black dots line) and after it (red line). The plot was obtained through the open source VSA.

3.2.2 Pre-processing of SSC measurements

Repeated SSC measurements in time using the sensor placed at the reference position (see *Section 3.1.3*) allowed knowing the linear relationship between SSC and time (i.e. the background increase). SSC measurements along the profiles were corrected, removing the background increase. SSC measurements in voltage were not converted to suspended solids concentration, because the calibration curve of NEP5000 sensors was still unknown. The SSC data analyses were performed with raw measurements in voltage, to maintain homogeneity in the data set for subsequent comparisons. Note that results and observations were not affected by the use of voltage, since the conversion had a linear dependence.

3.3 Data analyses

All the experimental data were elaborated in spreadsheet (Excel) and in Matlab. A statistical analysis was performed calculating average values ($\bar{x}$) of repeated measurements in time in the same points and standard deviations (σ), using *Equations 20-21*:

$$\bar{x} = \frac{1}{n}\sum_{i=1}^{n} x \qquad (20)$$

$$\sigma = \sqrt{\frac{1}{n-1}\sum_{i=1}^{n}(x-\bar{x})^2} \qquad (21)$$

where x is the repeated value measured in time. The Root Mean Square (RMS) relative error was determined to estimate and qualitatively compare the accuracy of theoretical and empirical relationships in describing velocity and SSC profiles. RMS relative error was calculated as:

$$RMS = \sqrt{\frac{1}{n}\sum_{i=1}^{n}\frac{(x_{o_i}-x_{e_i})^2}{x_{o_i}}} \quad (22)$$

where x_{o_i} is the observed value and x_{e_i} is the estimated value.

The methodology, used to fit theoretical values against velocity and SSC measurements, was a non-linear regression through the function in Matlab *nlinfit.m* (see *Figure 3.10*). The initial values of unknown parameters were estimated taking into account values from literature. In the next sections, equations used for velocity and SSC data analyses are described in detail.

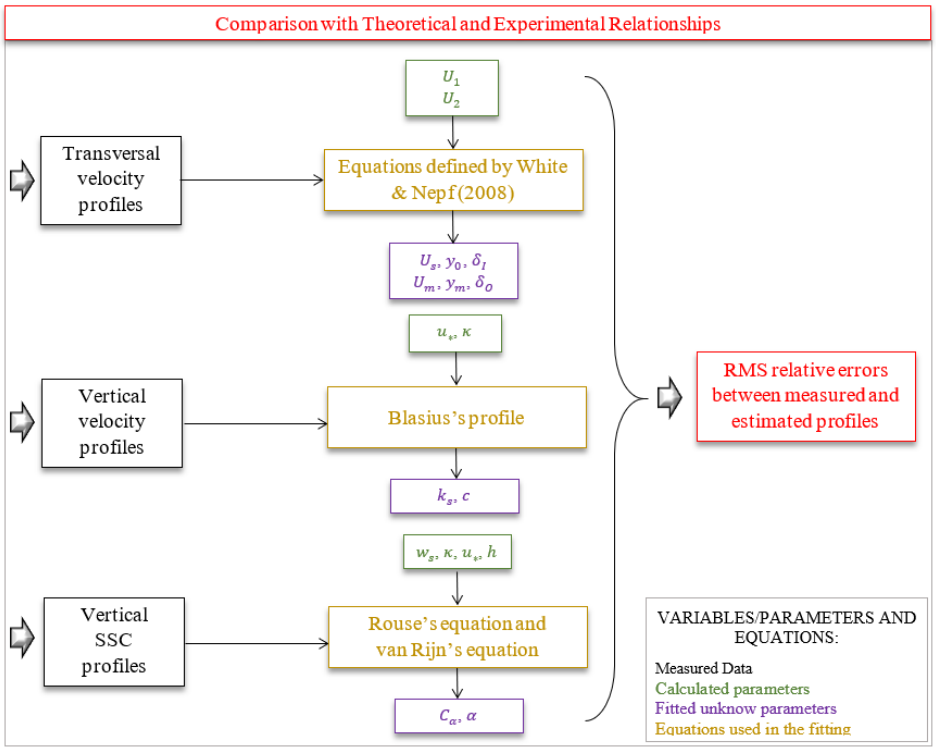

Figure 3.10: Visual scheme describing the methodology used in the comparison of measured data profile with theoretical and experimental equations. Comparisons were performed for the two vegetative conditions: foliated and leafless. Different colours underline which kind of variables, parameters and equations were used in the fitting.

3.3.1 Flow velocity field

As White & Nepf (2007; 2008) and Nepf (2012a) suggested, the transverse streamwise velocity profile can be divided in three different parts: a uniform profile characterized by a streamwise mean velocity U_1 within the vegetated patch, a hyperbolic tangent and parabolic profile at the vegetation interface for the presence of the shear mixing layer and a uniform profile characterized by a streamwise mean velocity U_2 in the open-channel (see *Figure 3.11*).

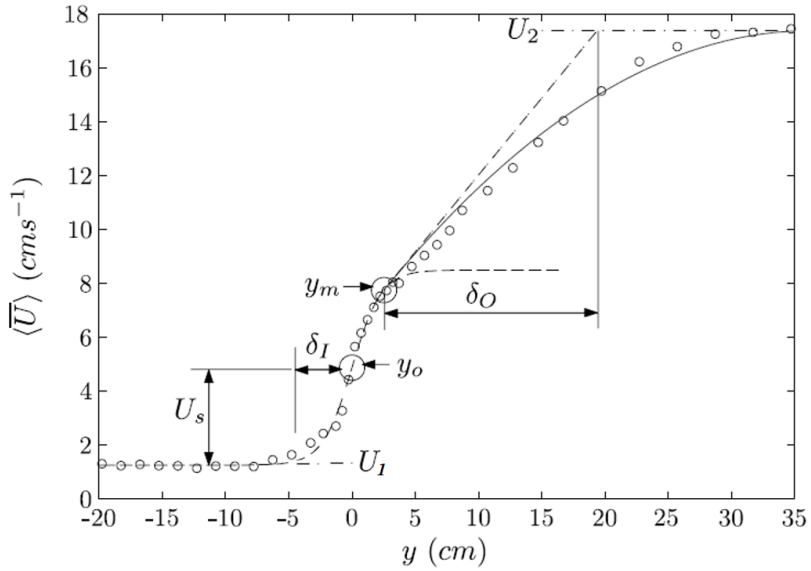

Figure 3.11: Representative streamwise transverse velocity profile in a partly vegetated channel. The main parameters shown are: penetration lengths of the shear mixing layer (δ_I, δ_O), inflection point (y_0), slope match point between two curves used in the inner and outer layer (y_m) and characteristic velocities (U_1, U_2, U_s). The vegetated patch is located where y coordinates are negative and the vegetation interface is placed at $y = 0$ cm (White & Nepf, 2008).

According to White & Nepf (2007; 2008), the two equations describing the transverse streamwise velocity profiles in the shear mixing layer can be fitted to measured profiles for both the vegetative conditions. In the inner layer (δ_I), the streamwise flow velocity ($\langle\overline{U}\rangle$) can be determined by the hyperbolic tangent profile:

$$\langle\overline{U}\rangle = U_1 + U_s\left[1 + tanh\left(\frac{y-y_0}{\delta_I}\right)\right] \quad (23)$$

where y is the transverse coordinate (m), y_0 is the location in which the lateral Reynolds stress is maximum (m) and U_s is the slip velocity. The unknown parameters in the fitting were U_s, y_0 and δ_I (see *Figure 3.10*). U_s is a property of δ_I and can be calculated as:

$$U_s = \langle\overline{U}\rangle(y_0) - U_1 \quad (24)$$

where $u(y_0)$ is the velocity observed at y_0 (m/s). In the outer layer (δ_O), the streamwise velocity distribution follows a profile very similar to the one obtained for a boundary-layer profile (i.e. parabolic profile under the assumption of a constant eddy viscosity, analogous of Poiseuille flow, even if the boundary layer is not laminar):

$$\langle\overline{U}\rangle = U_m + (U_2 - U_m)\left[\frac{y-y_m}{\delta_O} - \frac{1}{4}\left(\frac{y-y_m}{\delta_O}\right)^2\right] \quad (25)$$

where y_m is the location in the y axis where the slopes of *Equations 23-25* match (m) and U_m is the streamwise velocity observed at y_m ($U_m = u(y_m)$) (m/s). The unknown parameters in the fitting were U_m, y_m and δ_O (see *Figure 3.10*). U_1 and U_2 were determined calculating the time-average value of the streamwise velocity within the vegetation and in the open channel, respectively. As White & Nepf (2008) suggested,

plant-scale heterogeneity within the vegetated patch was removed, spatially-averaging the mean streamwise velocity over the vegetation spacing ($\Delta S = 0.177$ m).

The drag-density coefficient ($C_D a$) and the bed friction coefficient (c_f) were obtained through the balance (see *Equation 6*) between the drag (*Equation 9*) and the bed or surface gradient, assuming uniform and steady flow conditions and the contribution of the transverse shear stress (τ_{xy}) due to the lateral Reynolds stress as:

$$\tau_{xy} = -\rho\langle\overline{u'v'}\rangle \quad (26)$$

where u' and v' are turbulent fluctuations in x and y directions respectively (m/s). As White and Nepf (2008) and van Prooijen (2005) affirmed, the secondary circulation was always found one order of magnitude lower than the lateral Reynolds stress and, for this reason, neglected. The viscous contribution to the depth-averaged transverse shear stress was negligible due to the presence of high Reynolds numbers. Reynolds numbers, based on the flow depth (Re_h) and on the momentum thickness (Re_δ), were obtained through (White & Nepf, 2008):

$$Re_\delta = \frac{\rho(U_2 - U_1)\delta}{\mu} \quad (27)$$

$$Re_h = \frac{\rho U_2 h}{\mu} \quad (28)$$

where δ is the momentum thickness (m) and it was calculated through:

$$\delta = \int_{-\infty}^{\infty} \left[\frac{1}{4} - \left(\frac{\langle\overline{U}\rangle - (U_2+U_1)/2}{\Delta U}\right)\right] dy \quad (29)$$

where ΔU is the difference between U_2 and U_1 (m/s). Within the vegetation, the drag due to the presence of the bed was also neglected and *Equation 6* was simplified as:

$$\begin{cases} C_D a = \frac{2gS}{U_1^2} & vegetated\ area \\ c_f = \frac{2gSh}{U_2^2} & unvegetated\ area \end{cases} \quad (30)$$

The lateral shear velocity (u_*) was determined from the maximum lateral shear stress (White & Nepf, 2007):

$$u_*^2 = -\langle\overline{u'v'}\rangle_{max} = max\left(\frac{\tau_{xy}}{\rho}\right) \quad (31)$$

The vertical streamwise velocity profile, in unvegetated channels, can be described by a logarithmic distribution (*Blasius profile*) as shown in *Equation 32a.* The parameters of two logarithmic equations (*Equation 32a*) are linked by the relationship in *Equation 32b:*

$$\frac{\bar{u}}{u_*} = \frac{1}{\kappa}\ln\left(\frac{z}{z_0}\right) \quad \text{or} \quad \frac{\bar{u}}{u_*} = \frac{1}{\kappa}\ln\left(\frac{z}{k_s}\right) + c \quad (32a)$$

$$z_0 = k_s e^{-c\kappa} \quad (32b)$$

where $\bar{u}$ is the mean streamwise velocity in time (m/s), κ is the von Karman constant (~ 0.41), z is the vertical distance from the bed (m), z_0 is the hydrodynamic roughness length (m), k_s is the equivalent sand roughness (m) and c is the integration constant of the log law formula (m/s). *Equation 32a* was fitted to the measured velocity profile for both the vegetative conditions. The unknown parameters were k_s and c. According to Sukhodolov & Sukhodolova (2010) and Kouwen et al. (1969), in an unvegetated channel, the bed shear velocity could be calculated as:

$$u_* = \sqrt{\frac{\tau_0}{\rho}} = \sqrt{ghS_f} \qquad (33)$$

where τ_0 is the bed shear stress (N/m^2) and S_f is the friction slope (-), that can be equal to the slope of the free surface or the bed (S), if the Froude Number is lower than the unity ($Fr \ll 1$). In vegetated channel, *Equation 33* is not more valid, because the ratio $u_*/\sqrt{ghS_f}$ is less then 1. The bed shear stress (τ_0), within the vegetated patch, was calculated taking into account the presence of the emergent vegetation (Wu et al., 2005):

$$\tau_0 = \rho \frac{g n_c^2}{R_s^{1/3}} U_1^2 \qquad (34a)$$

where n_c is the Manning coefficient in the vegetation assumed as 0.03 and R_s is the spacing hydraulic radius defined as (e.g. Wu et al., 2005):

$$R_s = \frac{h\Delta s}{(2h+\Delta s)} \qquad (34b)$$

The vertical shear stress (τ_{xz}) was computed considering the contribution related to the vertical Reynolds stress as:

$$\tau_{xz} = -\rho\langle\overline{u'w'}\rangle \qquad (35)$$

where u' and w' are turbulent fluctuations in x and z directions respectively (m/s). The shear velocity was estimated from the maximum of the Reynolds stress, extrapolating its profile closed to the bed (τ_{xy_bed}) (Nepf, 2012a):

$$u_*^2 = -\langle\overline{u'w'}\rangle_{max} = max\left(\frac{\tau_{xz\_bed}}{\rho}\right) \qquad (36)$$

For both the streamwise velocity profiles (transversal and vertical), turbulence terms were calculated. The Turbulent Kinetic Energy[17] (TKE) was computed using the measured time series:

$$TKE = \frac{1}{2}\left(\overline{u'^2} + \overline{v'^2} + \overline{w'^2}\right) \qquad (37)$$

[17] Mean energy per unit of mass associated with turbulent eddies.

where $\overline{u'}$, $\overline{v'}$, $\overline{w'}$ are the velocity deviation components from the time-averaged velocity in the three directions (m/s). The turbulence intensity gave the level of turbulence and it was obtained by *Equation 38*:

$$I = \frac{\sqrt{\frac{1}{3}(\overline{u'^2}+\overline{v'^2}+\overline{w'^2})}}{\sqrt{\bar{u}^2+\bar{v}^2+\bar{w}^2}} = \frac{\sqrt{\frac{2}{3}TKE}}{U} \quad (38)$$

where $\bar{u}$, $\bar{v}$ and $\bar{w}$ are the time-average velocity components in x, y and z directions respectively (m/s) and U is the velocity magnitude (m/s).

3.3.2 Suspended sediment transport and net deposition

In the fully developed flow region, the advection process, within the vegetated patch, maintained a consistent role for a certain length scale (x_a) when the turbulence level is low. x_a was calculated through *Equation 39*, from the end of the diverging flow region (Zong & Nepf, 2011):

$$x_a = U_1 \frac{h}{w_s} \quad (39)$$

Due to the link between the settling velocity of particles and their characteristics (density, size and shape), x_a varied depending on the type of sediments used in the experiments. At a distance beyond x_a, sediment is transported mostly by diffusivity and the concentration of suspended sediment, collected within the vegetated patch, is lower than in the open-channel (Zong & Nepf, 2011). The length of the diverging flow region (x_D in *Figure 2.5*) was roughly estimated from longitudinal net deposition measurements within the vegetated patch. As reported by Zong & Nepf (2011), the longitudinal trend of net deposition has a little increase in the end of the diverging flow region. In the foliated condition, x_D~3 m from the leading edge, while, in the leafless condition, x_D~4 m from the leading edge.

In unvegetated channels, the vertical distribution of suspended sediment concentration (SSC) can be described by the Rouse's equation (Sharpe & James, 2006):

$$\frac{C}{C_\alpha} = \left(\frac{h-z}{z}\frac{\alpha}{h-\alpha}\right)^{w_s/\kappa u_*} \quad (40)$$

where C is the concentration of suspended particles at a certain height (g/l) and C_α is the reference concentration at height α above the bed (g/l). The reference level (α) has a large influence in the concentration profile very close to the bed. As noticed by van Rijn (1984), when α becomes very small ($\alpha < 0.01h$), the SSC profile can be affected by large errors. Even if α is not so small, the prediction of the SSC requires an error less than a factor of 2 and an error on the exponent of the Rouse's equation less than 20%, to have reliable results

(van Rijn, 1984). Assuming a parabolic-constant vertical sediment diffusivity distribution[18] with no damping effect, van Rijn's equation (*Equation 41*) can be used to predict vertical suspended sediment concentration distribution, in unvegetated channels. The SSC vertical profile is characterized by the Rouse's equation, for the first half of the water depth, and for a linear equation, for the other half (van Rijn, 1984):

$$\begin{cases} \frac{C}{C_\alpha} = \left(\frac{h-z}{z}\frac{\alpha}{h-\alpha}\right)^{w_s/\kappa u_*} & for\ \frac{z}{h} < 0.5 \\ \frac{C}{C_\alpha} = \left(\frac{\alpha}{h-\alpha}\right)^{w_s/\kappa u_*} e^{-4\frac{w_s}{\kappa u_*}\left(\frac{z}{h}-0.5\right)} & for\ \frac{z}{h} \geq 0.5 \end{cases} \quad (41)$$

In partly vegetated channels, *Equations 40-41* can be used to described the vertical SSC profiles in the open channel and at the vegetation interface (e.g. Sharpe & James, 2006). For this reason, *Equations 40-41* were used to fit the vertical measured SSC profiles (see *Figure 3.10*). The unknown parameters were C_α and α.

[18] For the first half of the water depth close to the bed, the vertical sediment diffusivity coefficient (ε_z) has a parabolic profile. For the second half, close to the free water surface, ε_z is constant.

4. Results and discussion

The characterization of the velocity field, the SSC transport and net deposition, regarding the fully developed flow region of the partly vegetated channel, is reported in the following sections. Comparative analyses of theoretical relationships and empirical prediction models are carried out for some velocity and SSC profiles (see *Section 4.4*). In *Section 4.5*, main uncertainties affecting accuracy of the results are pointed out, taking into account sensors resolution, measurements errors, pre-processing and data analyses errors propagation.

4.1 Characterization of the flow field

Average transverse and vertical velocity profiles, drag coefficients and turbulence levels are calculated and plotted in *Section 4.1.1-4.1.2*, for both vegetative conditions: leafless and foliated. Velocity data were normalized dividing by the maximum value of the transverse/vertical profile ($\langle\overline{U}\rangle_{max}$ and $\bar{u}_{max}$). The lateral and vertical Reynolds stresses were normalized dividing by the maximum value along the profile (Re_{xymax} and Re_{xzmax}) and the turbulent kinetic energy was divided by the shear velocity obtained through *Equation 31* for transverse profiles and through *Equation 36* for vertical ones.

4.1.1 Transverse velocity profile

Figure 4.1 shows the normalized streamwise velocity ($\langle\overline{U}\rangle$) profiles over the transect at a relative depth (z/h) of 0.56, for the leafless condition. In the open channel, there is a uniform streamwise velocity (U_2) that starts decreasing because of the higher drag experienced by the flow, close to the vegetation interface. The streamwise velocity (U_1) within the vegetated patch ($0 < \frac{y}{b} < 1$ in *Figure 4.1*) is not uniform as estimated from observations in previous works (e.g. White & Nepf, 2008; Nepf, 2012a). U_1 is affected by local deviations due to the presence of stems ($y/b = 0.24$ and $y/b = 0.78$). The drag-density parameter ($C_D a$) (see *Table 4.1*), calculated through *Equation 30*, is lower than the drag density of cylinders used in experiments carried out by White & Nepf (2008) and it is representative of the woody vegetation density that, commonly, can be found in nature. The drag-area parameter ($C_D ah$) is lower than 0.1 (see *Table 4.1*), the leafless vegetation can be described as sparse vegetation as assumed by Nepf (2012a). For sparse canopy the stem characteristic diameter (d) has a lower value than the stems spacing (Δs), so the turbulence is produced within stem wakes generating local disturbances (Nepf, 2012a).

Table 4.1: Variables and parameters calculated from measured velocity data, for leafless condition.

Variable	Value
U_1 (m/s)	0.406
U_2 (m/s)	0.679
$C_D a$ (m^{-1})	0.2
$C_D ah$ (-)	0.03
c_f (-)	0.012

Within the patch (at $y/b = 0.78$), the streamwise velocities of the two measured longitudinal positions (see *Figure 4.1*) differ because at $x = 11.285$ m the reading of the sensor was more affected by the presence of the stem than at $x = 11.535$ m. At the distance of 10 cm from the glass wall within the vegetation, the slight decrease in streamwise velocity is due to the presence of solid boundary (at $y/b = 1$).

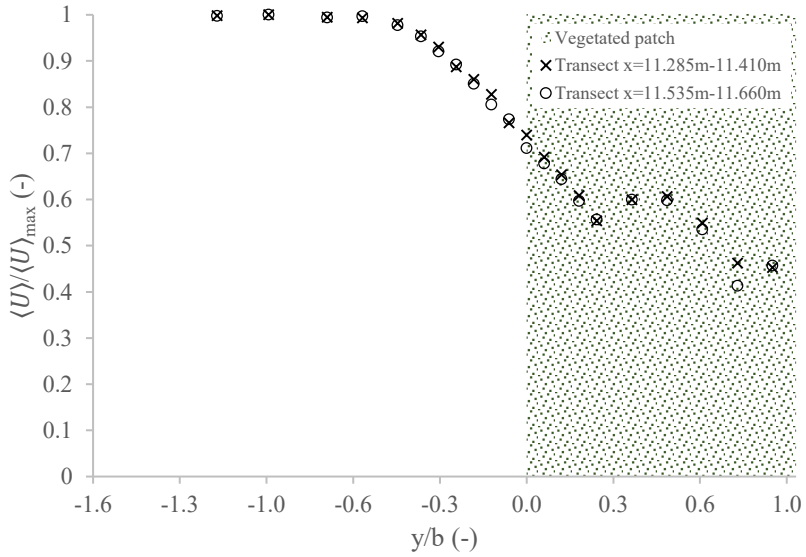

Figure 4.1: Transverse profiles of the normalized streamwise velocity for the leafless condition. The pattern fill represents the vegetated patch ($0 < \frac{y}{b} < 1$). All measurements were collected at a relative depth (z/h) of 0.56 from the bed.

The description of the turbulence (*Figure 4.2*), acting along the transverse streamwise velocity profile for the leafless condition, was determined using *Equations 26*, *37* and *38*. In all graphs of *Figure 4.2*, it is possible to observe an increasing trend getting closer to the vegetation interface and higher local fluctuation within the patch, compared to the one in the open-channel. The maximum lateral Reynolds stress (Re_{xymax}) was observed at the vegetation interface ($y/b = 0$) for both the transverse profiles. At $y/b = 0$, there is also the inflection point of the streamwise velocity profile (*Figure 4.1*), in agreement with the study of White & Nepf (2007) using emergent cylinders in a partly vegetated channel. As White and Nepf (2008) observed, for sparse vegetation, the shear mixing layer is quite symmetric with respect to the vegetation interface ($\delta_I \sim \delta_O$) and, in this area, lateral turbulent momentum transport is enhanced. Within the vegetated patch (at $y/b = 0.26$),

the lateral Reynolds stress presents (see *Figure 4.2a*) a negative value for both the longitudinal velocity measurements. These negative values were caused by the dynamical reconfiguration of the plant, as noticed by Siniscalchi et al. (2012).

As shown in *Figure 4.2b*, the normalized turbulent kinetic energy increases behind the stems. This fluctuation could be associated, according to Nepf et al. (2013), to the stem-scale turbulence generated by individual stems. The turbulent intensity (*Figure 4.2c*), as resulted in the experiments conducted by White & Nepf (2007), is enhanced within the vegetation compared to the open channel.

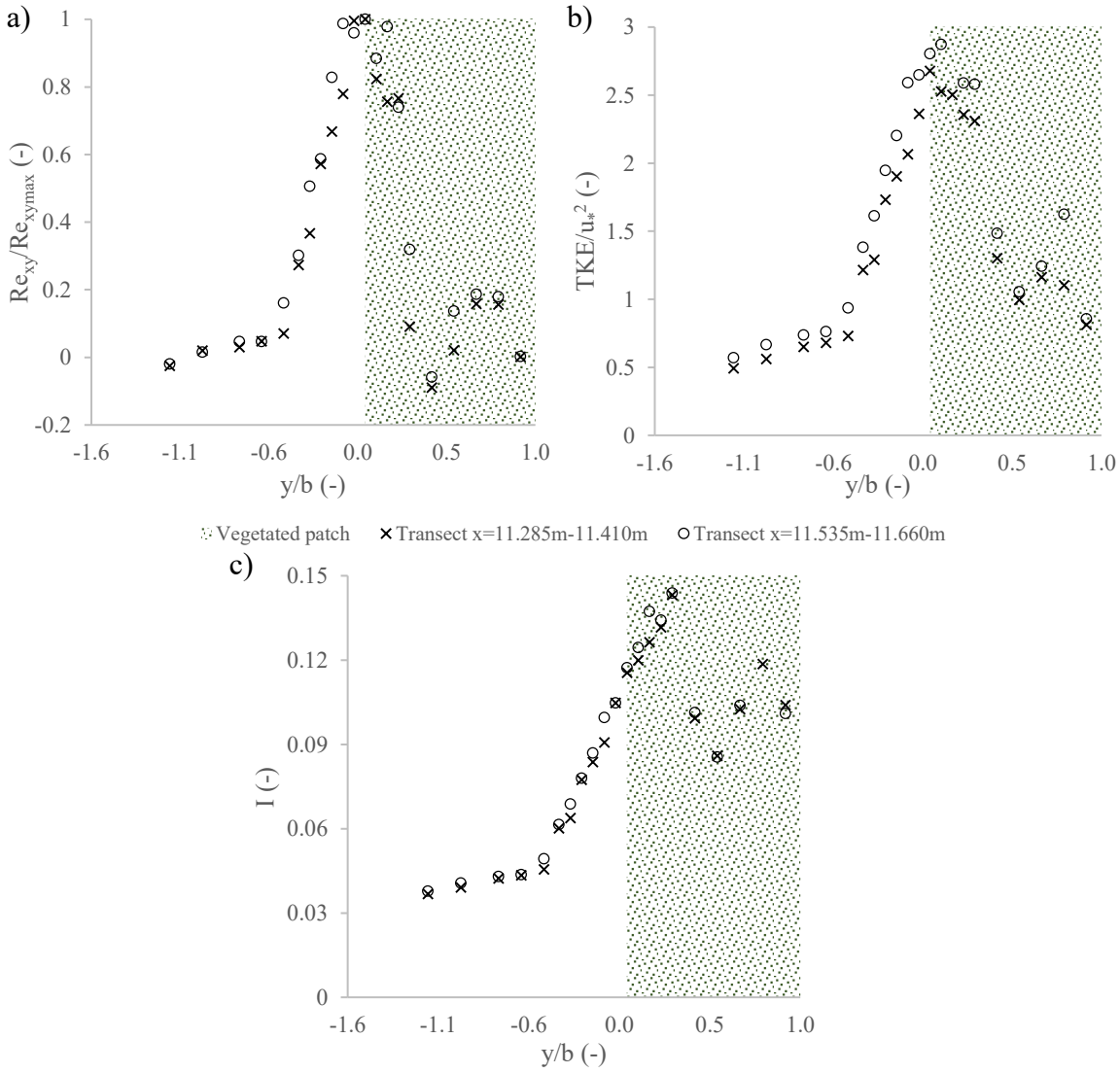

Figure 4.2: Turbulence terms acting on transverse streamwise velocity profiles for the leafless condition. a) Normalized lateral Reynolds stress, b) Normalized turbulent kinetic energy, c) Turbulence intensity. The pattern fill represents the vegetated patch.

Figure 4.3 shows the normalized streamwise velocity ($\langle \overline{U} \rangle$) profiles over the transects at a relative depth (z/h) of 0.56, for the foliated condition. As in the leafless condition, in the open channel, the streamwise velocity (U_2) is uniform, but it starts decreasing, further away from the vegetation interface, because of the higher drag experienced by the flow.

White & Nepf (2007), Zong & Nepf (2010) and van Prooijen et al. (2005) observed the same effect in the reduction of the streamwise velocity if the vegetation density increased. Within the vegetated patch, the streamwise velocity (U_1) is not uniform and it decreases. Due to the enhanced drag-density caused by the presence of the leaves (see *Table 4.2*), there is less local fluctuation in the vegetation than in the leafless case. The effect of the vicinity of the solid boundary within the vegetation is not detected in the foliated condition. According the division of Nepf (2012a) (see *Section 2.2.1*), the leafless vegetation can be described as transitional-to-dense vegetation because the drag-area parameter ($C_D ah$) is higher than 0.1 (see *Table 4.2*).

Table 4.2: Variables and parameters calculated from measured velocity data, for foliated condition.

Variable	Value
U_1 (m/s)	0.315
U_2 (m/s)	0.798
$C_D a$ (m^{-1})	0.7
$C_D ah$ (-)	0.13
c_f (-)	0.019

As observed by Nikora (2010) and Västilä & Järvelä (2017), increasing the drag-density parameter makes the streamwise velocity gradient enhanced, increasing the streamwise velocity in the open-channel and decreasing the one observed within the vegetated patch. In the outer layer (δ_O), the streamwise velocity does not vary consistently because it is less influenced by the vegetation density, as noticed by previous experiments using rigid emergent cylinders (e.g. White & Nepf, 2007). At the vegetation interface, the absolute values of the streamwise velocity increase with the increment of coherent vortex structure (Zong & Nepf, 2010). In the fully developed flow region, the streamwise velocity, in the shear mixing layer, remains constant, ranging between $0.5\ m/s$ and $0.7\ m/s$ in both the conditions (leafless and foliated).

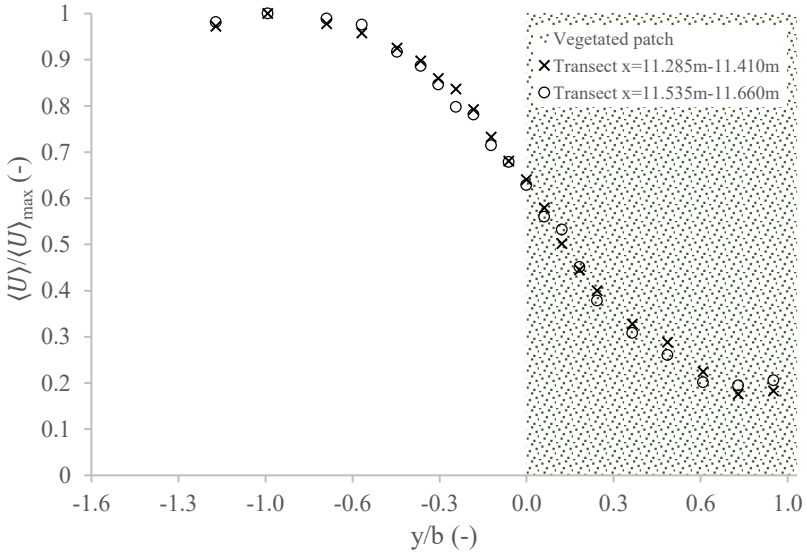

Figure 4.3: Transverse profiles of the normalized streamwise velocity for the foliated condition. The pattern fill represents the vegetated patch ($0 < \frac{y}{b} < 1$). Measurements were collected at a relative depth (z/h) of 0.56 from the bed.

In the partly vegetated channel with foliated condition, the turbulence (*Figure 4.4*) have an increase at the vegetation interface, as affirmed by White & Nepf (2007). For the foliated condition, the absolute magnitude of the lateral Reynolds stress values across the vegetation interface were about 4 times higher than the ones observed in the leafless condition. Re_{xymax} (see *Figure 4.4a*) is located some centimetres ($y/b \sim 0.13$) from the vegetation interface within the vegetated patch. White & Nepf (2008) noticed the deviation of the location of the maximum lateral Reynolds stress from the vegetation interface, when rigid cylinder arrays used in their experiments had a lower density.

Figure 4.4b shows the normalized turbulent kinetic energy for the foliated condition. At the vegetation interface, the normalized turbulent kinetic energy increases and, within the vegetation it has less fluctuations compared to the deviations in the leafless condition. In *Figure 4.4c*, the turbulence intensity presents, for the upstream transect (11.285 m-11.410 m), a trend very similar to the ones observed in leafless vegetation. While, for the downstream transect (11.535 m-11.660 m), the turbulence intensity remains high also near the glass wall and it is characterized by less fluctuation, likely caused by the different reconfiguration of leaves under the water flow. The turbulent intensity has higher values within the vegetated patch than in the open channel, as affirmed by White & Nepf (2007), and its magnitude increases when the vegetation density increases. The model defined by Nepf (1999) affirmed that the turbulence intensity decreased, increasing the plant density according to the decrease in the mean streamwise velocity within the vegetation. In the foliated case, the turbulent intensity has values double than in the leafless condition.

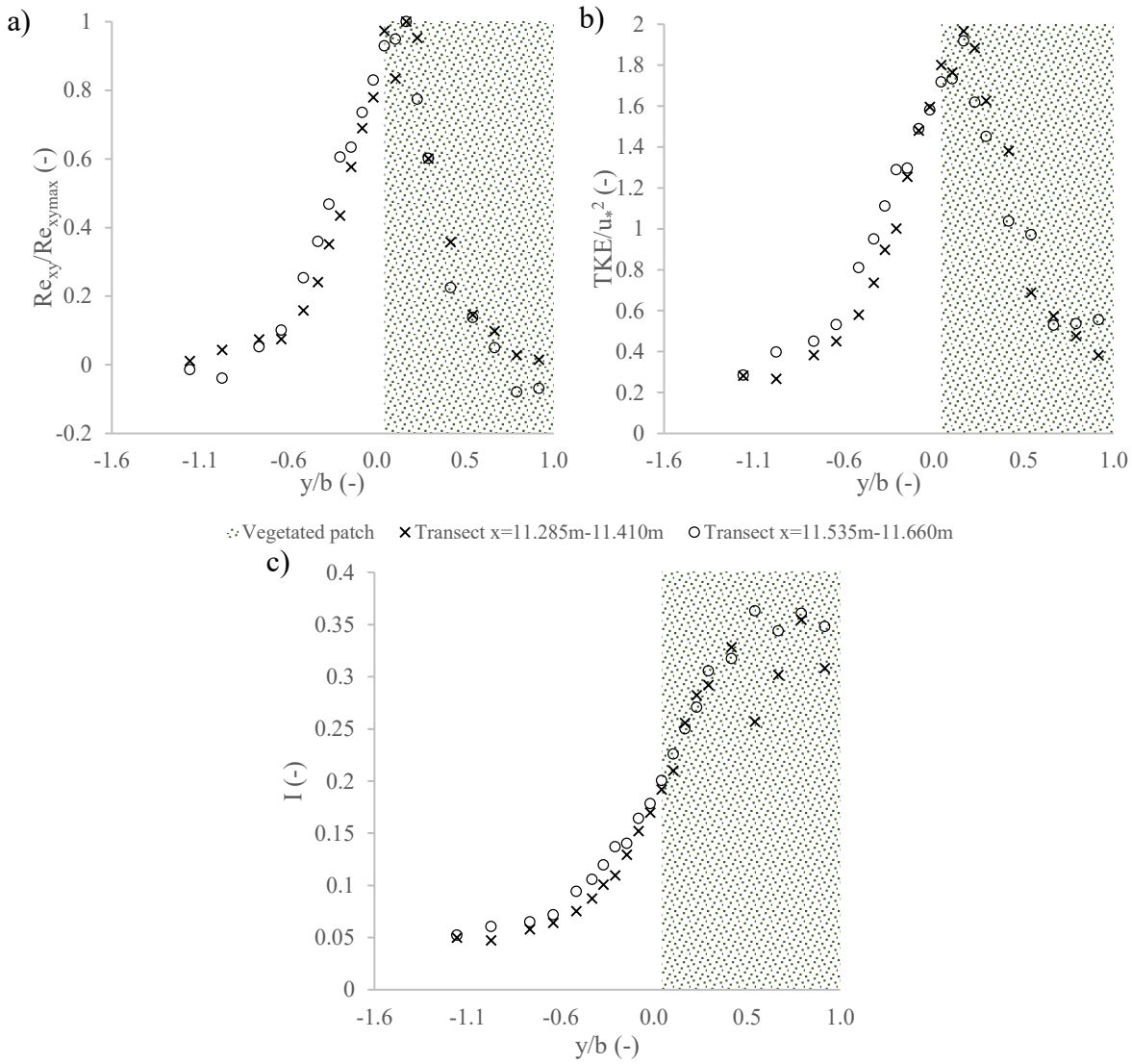

Figure 4.4: Turbulence terms acting on transverse profiles in the foliated case. a) Normalized lateral Reynolds stress, b) Normalized turbulent kinetic energy, c) Turbulence intensity. The pattern fill represents the vegetated patch.

4.1.2 Vertical velocity profile

The vertical streamwise velocity profiles (see *Section 3.1.3*) were collected at the longitudinal distance $x = 11.535m$ for three relative y coordinates: $y/b = -0.96$ (in the open channel), $y/b = 0$ (at the vegetation interface) and $y/b = 0.26$ (within the vegetated patch). In the leafless condition (*Figure 4.5*), the normalized streamwise vertical velocity profiles are characterized by the same trend: a sharp increase in the first layer above the bed and a very slight increase or constant profile close to the free water surface. Within the vegetation (*Figure 4.5c*), the profile starts decreasing sharply already at about half of the water level ($z/h = 0.5$), while, for the other profiles (*Figure 4.5a-b*), the variation is more gradual. Within the vegetation, there is the presence of the understory grass mat (height of 2 cm), that notably influences the results close to the bed. The vertical streamwise velocity

profile resembles, as Wu et al. (2005) and Vargas-Luna et al. (2015) noticed in their experiments using emergent rigid or flexible cylinders in partly vegetated channels, the typical Blasius logarithmic profile used to describe the vertical velocity profile in unvegetated open channel. This profile also agrees with the streamwise velocity profiles measured in sparse canopy (e.g. Nepf, 2012a). The absolute value of the streamwise velocity is higher in the open channel than at the interface and within the vegetation.

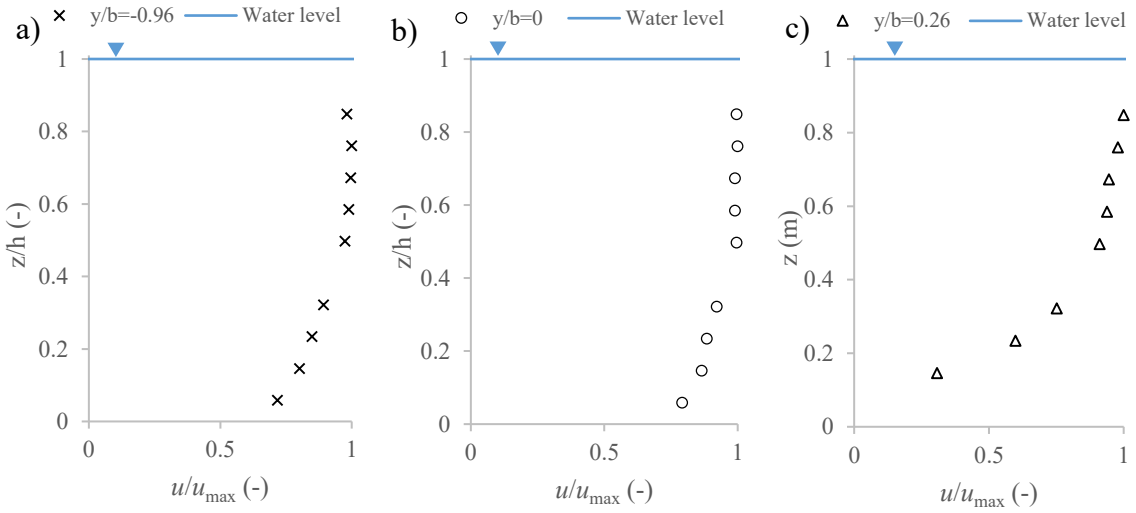

Figure 4.5: Vertical profiles of normalized streamwise velocity for the leafless condition: a) at a relative y coordinate $y/b = -0.96$ (in the open channel), b) at a relative y coordinate $y/b = 0$ (vegetation interface), c) at a relative y coordinate $y/b = 0.26$ (within the vegetated patch). Measurements were collected along the cross-section at x=11.535m.

In *Figure 4.6a*, the vertical Reynolds stress (Re_{xz}) presents higher fluctuation at the vegetation interface and within the vegetated patch, compared to the profile in the open-channel, for the leafless condition. In the open channel, normalized Re_{xz} profile follows the same trend of the one observed by Sukhodolov & Sukhodolova (2010) during their field experiments with emergent vegetation. Normalized Re_{xz} increases going from the free water surface to the bottom bed and it reaches its maximum value at a relative depth (z/h) of about 0.23. After the peak, normalized Re_{xz} decreases. At the vegetation interface, turbulence fluctuations due to vertical Reynolds stress and turbulent kinetic energy (*Figure 4.6a-b*) are higher than the ones observed for the other y locations, because they are enhanced by the coherent vortex structure in the shear mixing layer (see *Section 2.2.3*). The normalized turbulent kinetic energy (*Figure 4.6b*) increases going deeper in the open channel, while, within the vegetation it decreases close to the bed. *Figure 4.6c* shows the vertical profile of turbulence intensity. Within the vegetated patch, the turbulence intensity is enhanced compared to its profiles at the vegetation interface and in the open channel, mostly close to the bed, as also noticed by Luhar et al. (2008).

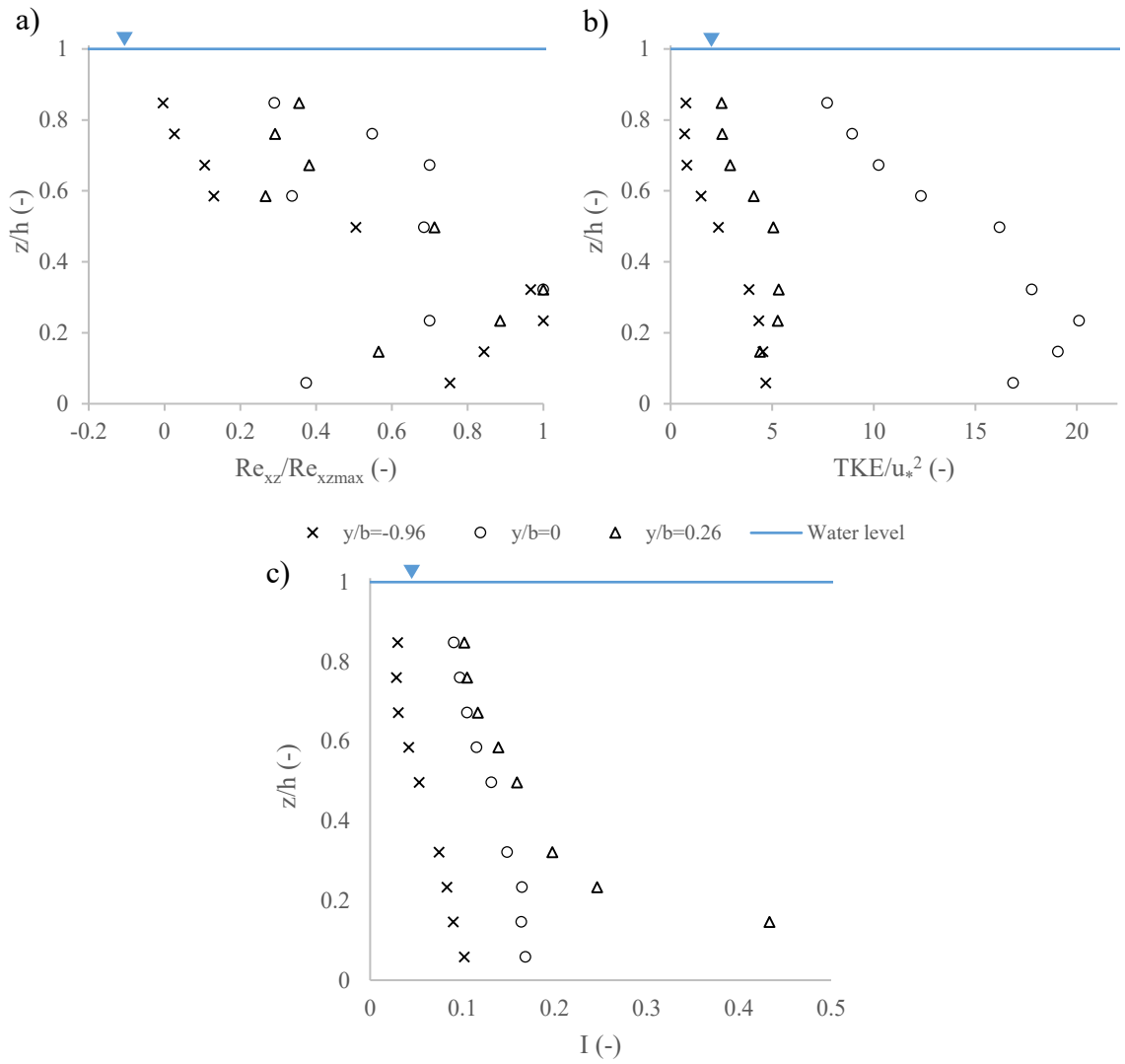

Figure 4.6: Turbulence terms acting on vertical profiles for the leafless condition. a) Normalized vertical Reynolds stress, b) Normalized turbulent kinetic energy, c) Turbulence intensity.

Figure 4.7 shows the normalized streamwise vertical velocity profiles for three relative y coordinates: $y/b = -0.96$ (in the open channel), $y/b = 0$ (at the vegetation interface) and $y/b = 0.26$ (within the vegetated patch), for the foliated condition. Trends are characterized by a sharp increase in the layer close to the bed, slight increase at about half of the water level and slight decrease close to the free water surface. The decreasing trend close to the free water surface is enhanced compared to the one noticed in the leafless condition (*Figure 4.5*), mostly for profiles at the vegetation interface and within the vegetation. Siniscalchi et al. (2012) observed the same decreasing trend for measured streamwise velocity profile in the open channel of a partly vegetated flow. Due to the presence of emergent plants, the inflection point at the top of the vegetation (e.g. Sukhodolov & Sukhodolova, 2010; Siniscalchi et al., 2012), typical of the streamwise velocity profile of submerged vegetation, was not observed.

The velocity magnitude decreases from the profile measured in the open-channel to the one measured within the vegetation. In the foliated condition, the velocity gradient across the

vegetation interface is higher (see *Section 4.1.1*). Due to the higher $C_D a$ in the foliated condition, the vertical streamwise velocity profile in the open channel has higher values than the one detected in the leafless condition. At relative position $y/b = 0.26$, the velocity magnitude is lower than the one measured in the leafless condition.

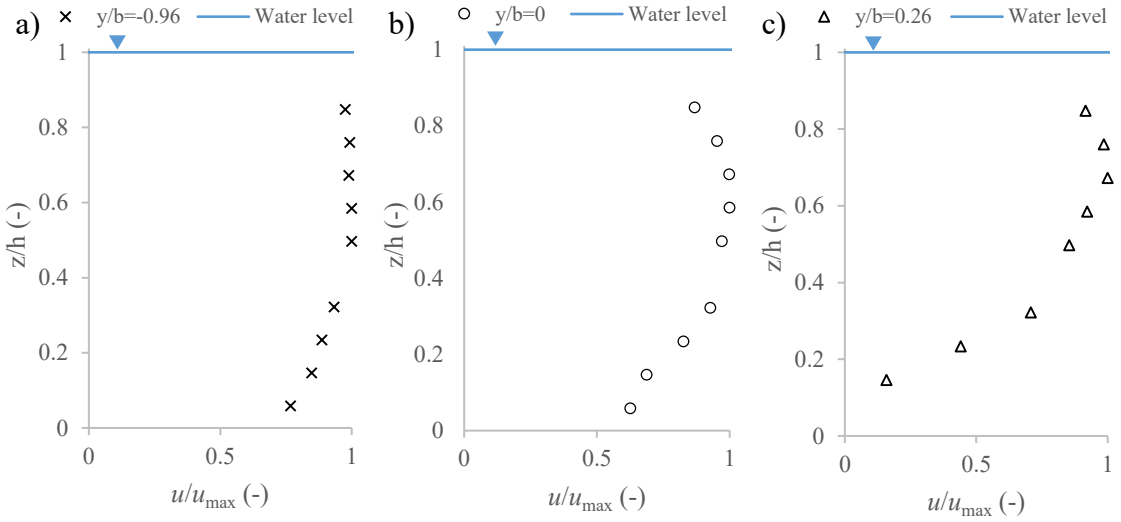

Figure 4.7: Vertical profiles of normalized streamwise velocity for the foliated condition: a) at a relative y coordinate $y/b = -0.96$ (in the open channel), b) at a relative y coordinate $y/b = 0$ (vegetation interface), c) at a relative y coordinate $y/b = 0.26$ (within the vegetated patch). All measurements were collected along the cross-section at x=11.535m.

In the foliated condition, the vertical Reynolds stress (*Figure 4.8a*) increases down from the water surface until the maximum value at around relative depth $\frac{z}{h} = 0.32$. After the peak, Re_{xz} decreases sharply for the vertical profiles at the vegetation interface and within the patch and slightly for the profile in the open-channel. Negative values of Re_{xz} are observed in vertical profiles at relative positions $y/b = 0$ and $y/b = 0.26$, due to the reconfiguration and movement of leaves under the flow, in agreement with the observations by Siniscalchi et al. (2012) in their experiments. Luhar et al. (2008) noticed that, within the vegetation, the shear stress close to the bed is reduced compared to the one in the open channel. The vegetative drag, within the vegetated patch, plays the main role.

The normalized turbulent kinetic energy (*Figure 4.8b*) has the same trend as the one observed for the leafless condition, but the magnitude is higher in the foliated case. The turbulence intensity (*Figure 4.8c*) is enhanced within the vegetation, mostly next to the bed, and its values are, as for the turbulent kinetic energy, higher than in the leafless condition.

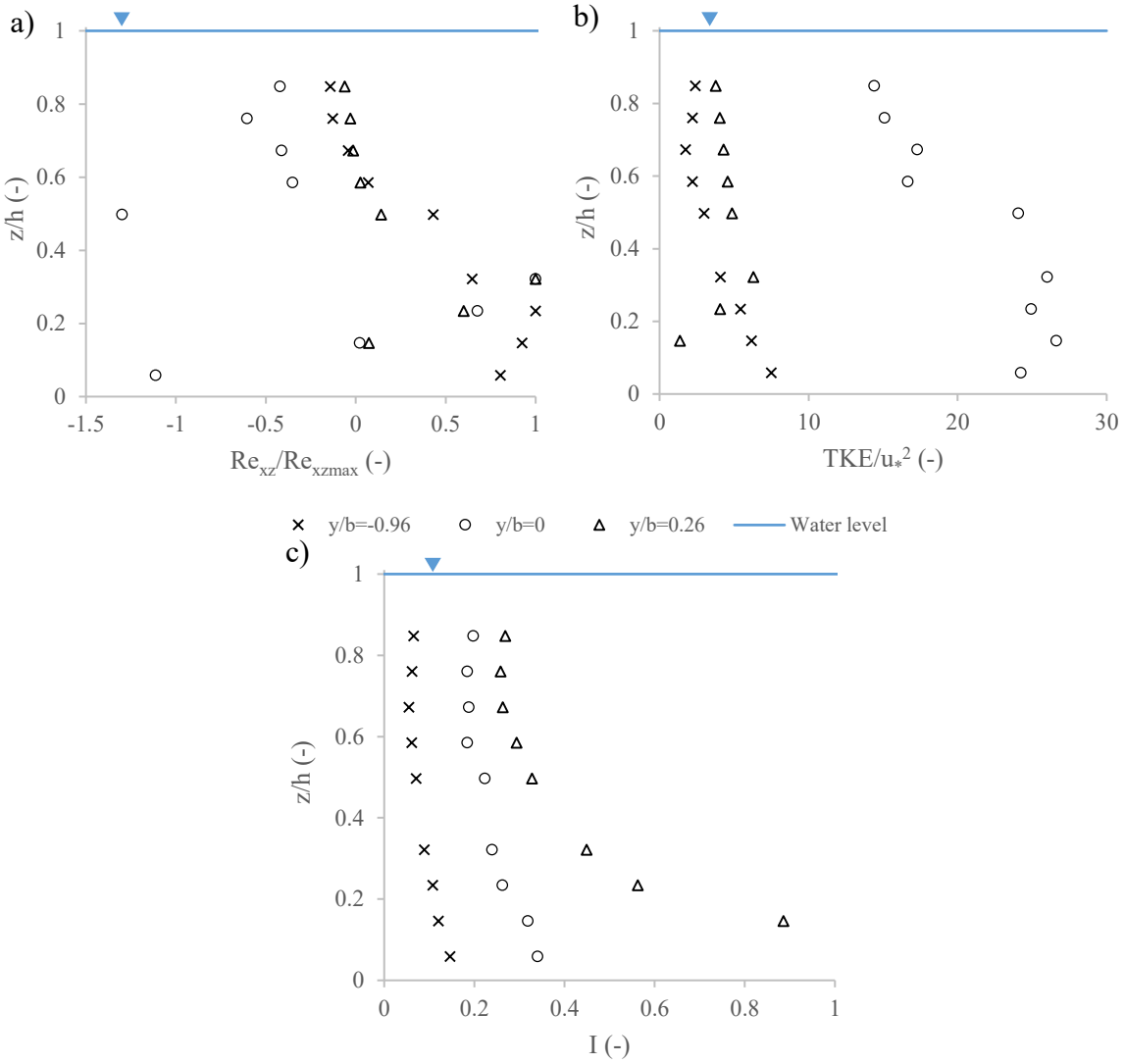

Figure 4.8: Turbulence terms acting on vertical profiles for the foliated condition. a) Normalized vertical Reynolds stress, b) Normalized turbulent kinetic energy, c) Turbulence intensity.

4.2 Characterization of suspended sediment transport

Average of turbidity measurements in transverse and vertical profiles were calculated and plotted in *Sections 4.2.1-4.2.2*, for both conditions: leafless and foliated vegetation. SSC data in transverse profiles were normalized dividing by the SSC value measured at the reference point (V_{SSCref}) (see *Section 3.1.3*), SSC data in vertical profiles have been normalized dividing by the maximum value of the profile (V_{SSCmax}). Note that SSC values are left in voltage (see *Section 3.2.2*). Due to the linearity of the conversion between SSC and voltage, observations and normalized trends are assumed to be valid.

4.2.1 Transverse SSC profile

Figure 4.9 shows SSC transverse profiles for the leafless case in the fully developed flow region. In the open channel, the turbidity increases from the glass wall to the middle of the channel and, across the vegetation interface, it starts slightly decreasing. The decrease next to the glass wall, in the open channel, is due to the lower streamwise velocity affected by the solid boundary layer. Within the vegetated patch, the SSC transverse profile does not decrease from the vegetation interface, as Zong & Nepf (2011) observed in their experiments around a finite patch of rigid cylinders, but it slightly increases. The upstream cross-section profile presents a very high turbidity in the first measurement points next to the glass wall within the vegetation. These measurements are clearly affected by the presence of the stem (relative position in y axis at $y/b = 0.78$) in the sampling volume of OBS3+ sensor. Sampling points were located behind the stem.

The normalized suspended sediment concentrations within the vegetation and in the open channel, are characterized by very similar values. This similarity is due to the contribution of the advection term in the transport process. For sparse vegetation ($C_D aH \ll 0.1$), as affirmed by Nepf (2012a), the erosion and sediment transport are enhanced. The advection length (x_a), obtained through *Equation 39,* is equal to 8.5 m from the end of the diverging flow region. The two cross-sections measured for SSC were still within x_a. In *Figure 4.9*, the normalized SSC values measured along the upstream cross-section are higher than the ones measured in the downstream cross-section. This result is in agreement with the decrease of SSC in longitudinal direction, in the fully developed flow region, as reported by Västilä & Järvelä (2017) and Zong & Nepf (2011).

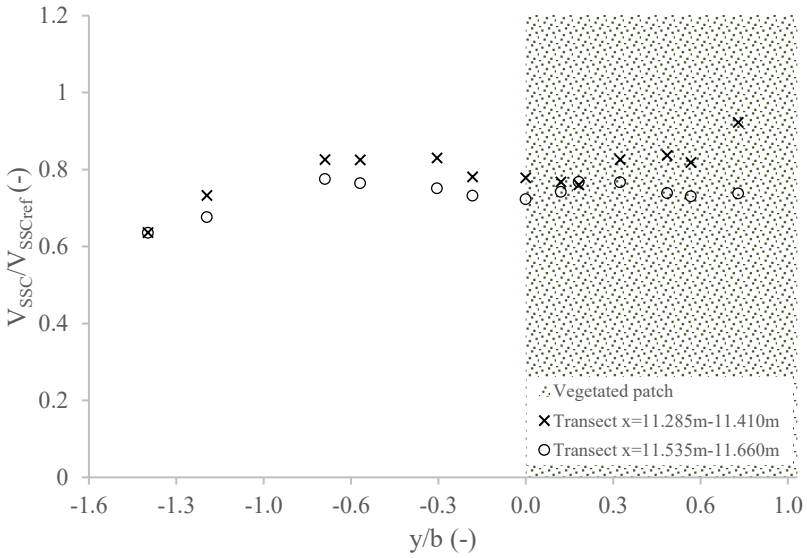

Figure 4.9: Transveres profiles of normalized suspended sediments concentration for the leafless condition. The pattern fill represents the vegetated patch. Measurements are collected at a relative depth of $z/h = 0.56$ from the bed.

Figure 4.10 shows the normalized SSC transverse profiles for the foliated condition. In the open channel, SSC increases sharper than in the leafless case, from the glass wall. This enhancement in the open channel is due to the presence of higher streamwise velocity in the foliated condition compared to the one observed in the leafless condition. Close to the vegetation interface, SSC starts decreasing. There is a net distinction in the area within the vegetation very close to the interface, in which the turbidity keeps longer the concentration of suspended sediment than in the other part of the patch where the concentration is lower and particles tend to settle. Due to the higher density ($C_D ah > 0.1$), more particles settle, as noticed by Västilä & Järvelä (2017) and Nepf (2012a). The advection length is equal to 6.5 m from the end of the diverging flow region. The two cross-sections are not within x_a and the advection term is not able to transport suspended sediment as in the open channel. In agreement to the experiments performed by Zong & Nepf (2011), SSC decreases in longitudinal direction.

The higher density, due to the presence of leaves, determined a reduction in the thickness of the inner layer within the vegetated patch, as reported in *Section 4.1.1*. The penetration of shear mixing vortices and the lateral transport are, consequently, reduced.

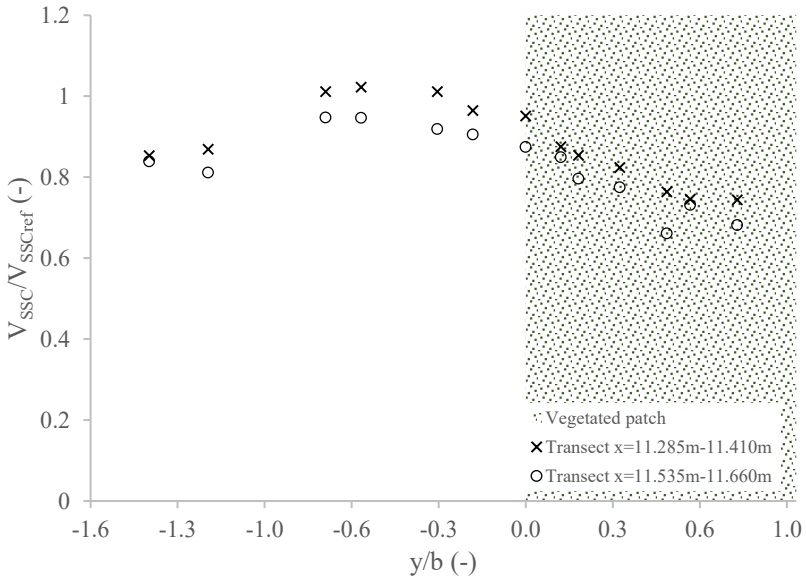

Figure 4.10: Transveres profiles of normalized suspended sediments concentration for the foliated condition. The pattern fill represents the vegetated patch. Measurements are collected at a relative depth of $z/h = 0.56$ from the bed.

4.2.2 Vertical SSC profile

Vertical SSC profiles were collected at the longitudinal distance $x = 11.535m$ for five relative y coordinates: two in the open channel ($y/b = -0.96$ and $y/b = -0.3$), one at the vegetation interface ($y/b = 0$) and two within the vegetation ($y/b = 0.26$ and $y/b = 0.78$). For the leafless condition, in the open-channel and at the vegetation interface (*Figure 4.11a*), SSC increases going deeper: slightly close to the free water surface and

sharply close to the bed. This profile is comparable to the ones observed by Zheng et al. (2013) and van Rijn (1984) in unvegetated channels. Sharpe & James (2006), in experiments on net deposition using rigid cylinders in a partly vegetated flume, assumed the use of theoretical equations, defined for unvegetated channel, for the description of the vertical SSC profile at the vegetation interface. At the vegetation interface, the highest relative SSC value is likely due to the disturbance caused by the presence of the grass mat (see *Section 3.1.3*).

Within the vegetation (*Figure 4.11b*), measured SSC profiles have different trends. At relative position $y/b = 0.26$, SSC has a gradual decrease close to the free water surface and an increase approaching the bottom bed. At relative position $y/b = 0.78$, there are more fluctuations and SSC tends to decrease in greater water depths. These opposite trends are caused by local disturbances and turbulence generated at stem scale (e.g. Nepf, 2012a). In sparse cylinder-shape elements, the characteristic diameter of the stems is lower than the spacing of stems, so the turbulence is produced by stem wakes (see *Section 4.1.1*). Measurement points affected by the presence of the vegetation, were shifted downstream from the stems. At $y/b = 0.78$, the stem is closer than at $y/b = 0.26$ and the fine sediment experiences higher level of turbulence close to the bed. In this area, sedimentation is reduced and sediment transport enhanced, according to Västilä & Järvelä (2017).

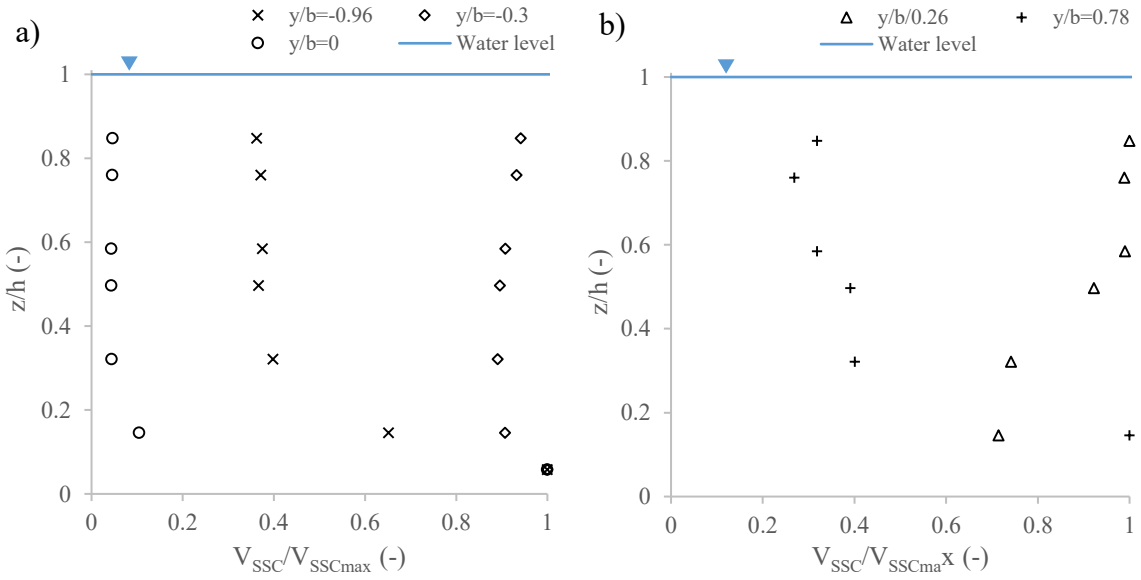

Figure 4.11: Vertical profiles of normalized suspended sediments concentration for the leafless condition: a) open-channel and vegetation interface; b) within the patch. Measurements were collected along the cross-section at x=11.535m.

Figure 4.12 shows normalized SSC vertical profiles in the open channel ($y/b = -0.96$ and $y/b = -0.3$), at the vegetated interface ($y/b = 0$) and within the vegetation ($y/b = 0.26$ and $y/b = 0.78$), for the foliated condition. In the open channel and at the vegetation interface (*Figure 4.12a*), SSC vertical profiles are similar to the ones obtained for the leafless condition, presenting more fluctuations in some sampling points. SSC increases slightly in the layer close to the free water surface and sharply close to the bed, as the SSC

vertical profile observed by van Rijn (1984) for unvegetated channels. At the vegetation interface ($y/b = 0$), the measured point closest to the bed is affected by the presence of the grass mat in the sampling volume of the sensor.

Figure 4.12b shows normalized SSC vertical profiles within the vegetation for the foliated condition. The two profiles (at $y/b = 0.26$ and at $y/b = 0.78$) are similar: SSC decreases down from the water surface until half of the water depth ($z/h = 0.5$). In the layer close to the bed SSC starts increasing. The SSC vertical profiles have an opposite trend compared to the one of the vertical streamwise velocity: when SSC decreases, the streamwise velocity increases and vice versa.

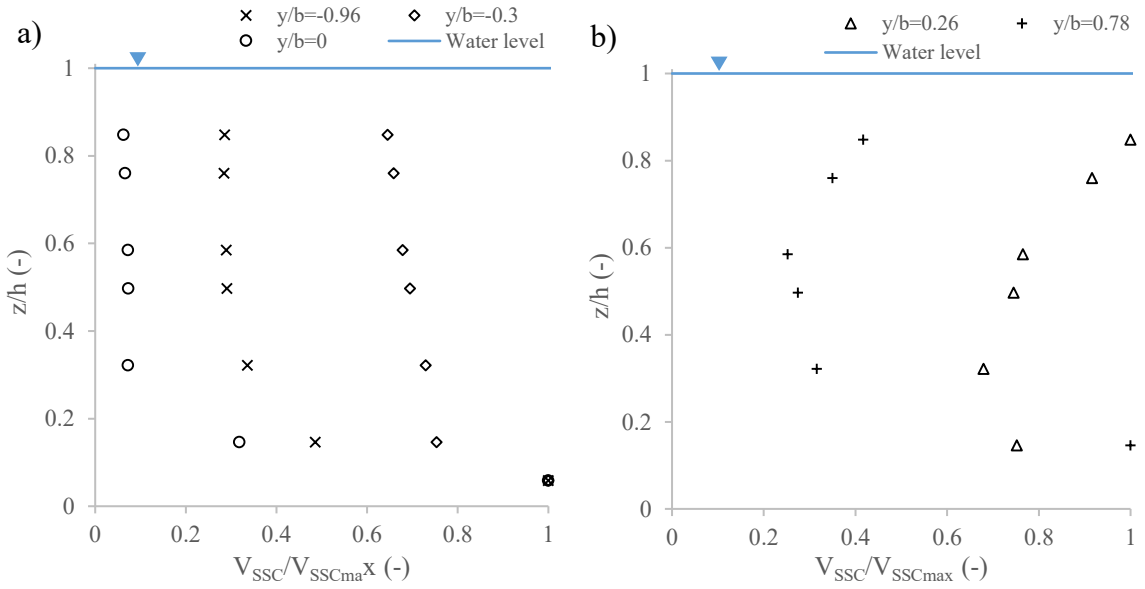

Figure 4.12: Vertical profiles of normalized suspended sediments concentration for the foliated condition: a) open-channel and vegetation interface; b) within the patch. Measurements were collected along the cross-section at x=11.535m.

For both vegetative conditions, normalized SSC values for the profile close to the vegetation interface ($y/b = 0.26$) are higher than values for the profile further ($y/b = 0.78$). This observation was also described by Zong & Nepf (2011) in their experiments in partly vegetated channel. Normalized SSC values, measured in the foliated condition, are higher than the one observed in the leafless condition in the open-channel, while, they are lower within the vegetated patch. According to Nepf (2012a), dense vegetation (foliated) enhances deposition and reduces sediment transport, while, sparse vegetation (leafless) enhances erosion and sediment transport.

4.3 Net deposition

Average of net deposition measurements in transverse profiles have been calculated for both conditions: leafless and foliated vegetation. Normalized values of net deposition were calculated by dividing the transverse profile value with the maximum value. For both

vegetation conditions, the transverse net deposition profile, in the open–channel, is characterized by very low values. The net deposition is about 4% of the one detected within the vegetated patch along the same cross-section and, for this reason, neglected from the graphs in *Figure 4.13*. The enhancement in settling, within the vegetation, is confirmed by the study on particle settling velocity within emergent vegetation performed by Elliott (2000). The presence of streamwise velocity gradient between the open channel and the vegetated patch, linked to the different drag, is the main cause of the difference in net deposition measurements between the open channel and within the vegetation. In the fully developed flow region, Abt et al. (1994), Västilä & Järvelä (2017) and Zong & Nepf (2010; 2011) observed enhanced net deposition within the vegetation and very low values in the open channel. In the outer layer (δ_o), for both vegetative conditions, the net deposition was negligible, due to the higher turbulence caused by the presence of the coherent vortices.

In the leafless and foliated condition, the net deposition profiles (*Figure 4.13*) have a maximum value very close to the vegetation interface and the trend decreases entering in the vegetated patch, according to observations performed by Sharpe & James (2006) and Zong & Nepf (2011) in laboratory experiments. In leafless condition (*Figure 4.13a*), in the upstream cross-section (at $x = 10.00\ m$), the net deposition does not decrease for the measurement points further away from the vegetation interface. This uniformity in net deposition measurements outside the inner layer (δ_I) is due to the advection term in the transport process (see *Section 4.2.1*). In the foliated condition (*Figure 4.13b*), the extension of the decreasing in net deposition increases, within the vegetation, due to the higher drag-density parameter (see *Section 4.1.1*), as also observed by Zong & Nepf (2011). In this vegetative condition, the advection length does not include the two cross-sections measured (see *Section 4.2.1*).

According to the field experiments conducted by Västilä & Järvelä (2017), the absolute values of the net deposition in the foliated condition are, within the vegetated patch, higher than in the leafless condition. This is due to the difference in streamwise velocity gradient, in agreement with Sharpe & James (2006), and in the turbulence penetration, strictly linked to variation of the vegetation density (e.g. Nepf, 2012a).

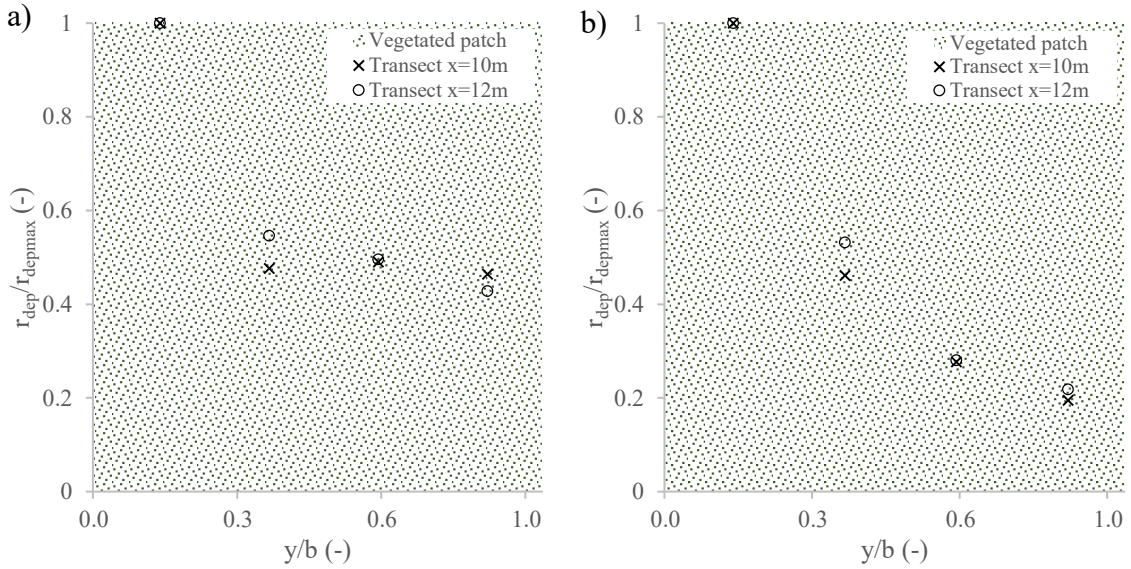

Figure 4.13: Normalized transverse net deposition profiles within the vegetated patch in: a) leafless condition, b) foliated condition. The pattern fill represents the vegetated patch.

Within the vegetated patch, the net deposition decreases from upstream cross-section to the one downstream in the leafless condition (see *Table 4.3*). The reduction in net deposition in the longitudinal direction, for the fully developed flow region, was also observed by Zong & Nepf (2010), Schmid et al. (2005) and Sharpe & James (2006). In the experiments they used emergent rigid cylinders that had morphology and biomechanics similar to the reeds or grass, not properly to the artificial emergent flexible natural-like vegetation used in this study. In the foliated condition (see *Table 4.3*), a slight increase from the upstream cross-section to the downstream one was detected, unlike observations performed by Västilä & Järvelä (2017) from experiments on field with natural plants. They, indeed, noticed a reverse relationship between distance from the seeding point and magnitude of the net deposition. The unexpected increase in leafy vegetation could be due to the enhanced mechanical dispersion, as Nepf (2012a) suggested.

Table 4.3: Results of mean net deposition values (g/s) and standard deviations (g/s), for leafless and foliated conditions. A, B, C, D are four grass strips formed the patch at x=10m and x=12m; A is the strip near the glass wall, D is the strip near the vegetation interface.

	Leafless condition		Foliated condition	
y\x	10 m	12 m	10 m	12 m
A	$9.17*10^{-4}\pm1.78*10^{-4}$	$4.86*10^{-4}\pm1.19*10^{-4}$	1.04*10-3±1.19*10^{-4}	$1.37*10^{-3}\pm1.86*10^{-4}$
B	$9.69*10^{-4}\pm1.91*10^{-4}$	$5.64*10^{-4}\pm1.36*10^{-4}$	$1.48*10^{-3}\pm2.5*10^{-4}$	$1.77*10^{-3}\pm2.03*10^{-4}$
C	$9.42*10^{-4}\pm1.91*10^{-4}$	$6.19*10^{-4}\pm1.81*10^{-4}$	$2.47*10^{-3}\pm4.97*10^{-4}$	$3.35*10^{-3}\pm5.33*10^{-4}$
D	$1.98*10^{-3}\pm5.19*10^{-4}$	$1.14*10^{-3}\pm2.38*10^{-4}$	$5.36*10^{-3}\pm9.06*10^{-4}$	$6.31*10^{-3}\pm6.81*10^{-4}$

4.4 Applicability of theoretical and empirical equation

In laboratory and on field experiments the characterization of the flow field in partly vegetated channels is quite well developed for transverse profiles (e.g. White & Nepf,

2008; 2007; Sukhodolov & Sukhodolova, 2010) and vertical profiles (e.g. Siniscalchi et al., 2012; Nikora et al., 2013). The complexity characterizing natural vegetation in terms of species distribution, properties and structure (see *Section 2.1*), makes hard the generalization of findings and equations derived from a certain setup or flow field that may not be reliable in other conditions. The vertical SSC profile equations describing the transport of suspended sediment derive mostly from studies in unvegetated channel (e.g. van Rijn, 1984) and they are quite used also in partly vegetated flows for vertical SSC profile in the open channel and at the vegetation interface (e.g. Sharpe & James, 2006; Wu et al., 2005). In the next sections, some of theoretical and empirical equations (see *Figure 3.10*) are applied to vertical and transverse profiles of velocity and SSC measurements.

4.4.1 Velocity profiles

The transverse streamwise velocity profile (see *Equations 23-25*), used by White & Nepf (2008), describes the velocity pattern across the vegetation interface, not considering the effects of the reduction of velocity magnitude near the two solid boundaries of the flume. Measurement points, next to the glass wall within the vegetation, were, therefore, neglected during this test of applicability.

Figure 4.14 shows transverse profiles of normalized measured and modelled streamwise velocity, divided by the uniform velocity in the open channel (U_2), for the leafless and foliated conditions. In the leafless condition (see *Figure 4.14a*), the modelled curve follows very well the pattern of velocity measurements. The Root-Mean-Square (RMS) relative error is equal to 0.97%, meaning that a vortex-based model of velocity and shear mixing stress (e.g. White & Nepf, 2008) can be used to estimate the streamwise velocity across the vegetation interface when the vegetation is characterized by the stems (winter/autumn period). In the foliated condition (see *Figure 4.14b*), the modelled profile fits very well the measured velocity at the vegetation interface. However, the streamwise velocity in the open channel and within the vegetation is not uniform as the profile assumed by White & Nepf (2008). In the open channel, there is a measured point ($y/b = 0.96$) that differs from the uniform value U_2 (see *Figure 4.14b*). Within the vegetation, the streamwise velocity continues decreasing instead of staying uniform and equal to U_1 (see *Figure 3.11*). Due to deviations in the streamwise velocity in the open channel and within the vegetation, the RMS relative error is higher than the one resulted in the leafless condition. The error is equal to 11%, very close to threshold value of 10%, so the model is still reliable in the prediction of the transverse streamwise velocity in partly vegetated channel characterized by woody foliated emergent vegetation (spring/summer period).

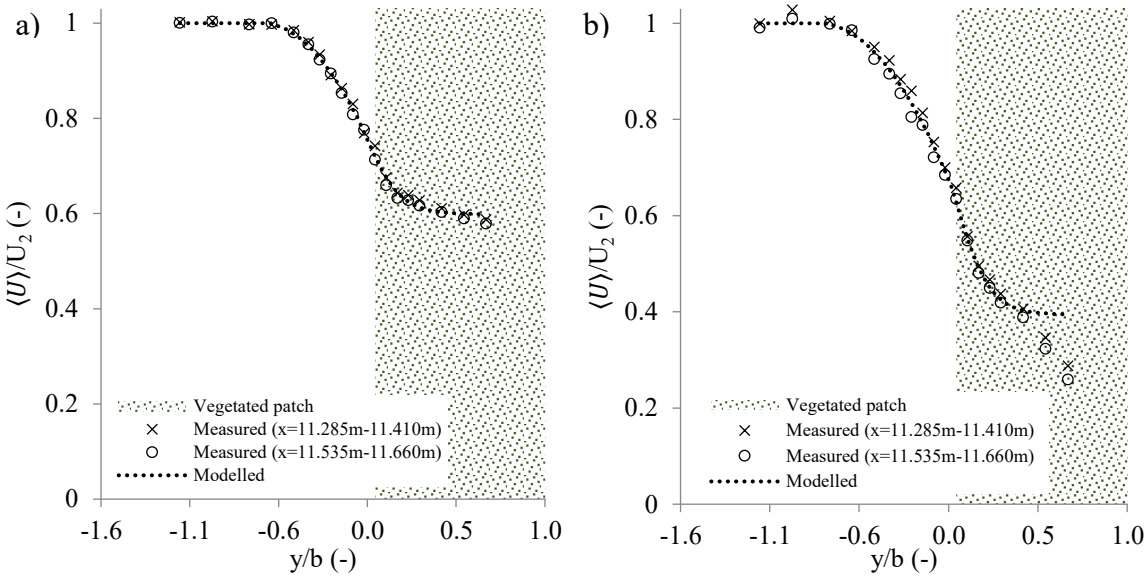

Figure 4.14: Measured and modelled transverse profiles in: a) leafless condition, b) foliated condition. The pattern fill represents the vegetated patch. The measured data are laterally averaged within the vegetation using a filter of window length equal to the stem spacing.

Table 4.4 shows parameters and variables measured, calculated and fitted using the *Equations 23-25* in *Section 3.3.1* for the transverse streamwise profiles, in both vegetative conditions. The streamwise velocity gradient between the streamwise velocity in the open channel (U_2) and the streamwise velocity within the vegetation (U_1) increases in the foliated condition, as shown in *Table 4.4*. In the foliated condition, the maximum lateral Reynolds stress was found at the vegetation interface, while, in the leafless condition, it was determined at a distance of 2 cm from the interface (see y_0 in *Table 4.4*). This shift was also noticed in the study of White & Nepf (2008) in a partly vegetated channel with vegetation characterized by rigid cylinders. The viscous stress was neglected (see *Section 3.3.1*) from the momentum balance, because of the high Reynolds numbers ($O(10^4 - 10^5)$), calculated based on the momentum thickness (Re_δ) and on the flow depth (Re_h) (see *Equations 27-28*).

Table 4.4: Experimental parameters and results from the fitting for both vegetative conditions (leafless, foliated), in the transverse streamwise velocity profiles.

Variable	Leafless condition	Foliated condition
U_1 (m/s)	0.406	0.315
U_2 (m/s)	0.679	0.798
U_s (m/s)	0.112	0.182
U_m (m/s)	0.556	0.553
y_0 (m)	0.057	0.071
y_m (m)	0.04	0.055
δ_i (m)	0.047	0.045
δ_o (m)	0.062	0.085
δ (m)	0.028	0.033
Re_δ (-)	$7.66*10^4$	$1.60*10^4$
Re_h (-)	$1.16*10^5$	$1.36*10^5$

To determine the vertical streamwise velocity profile, the shear velocity (u_*) was calculated through *Equation 36*. Within the vegetation, another approach was performed for the calculation of the bed shear stress (see *Equation 34a*) following Wu et al. (2005). The shear velocity, determined by *Equation 33*, did not give reliable results in the prediction of the vertical streamwise profiles and it is not reported in the fitting in *Figure 4.15*.

Figure 4.15 shows vertical profiles of normalized measured and modelled streamwise velocity, divided by the maximum velocity for each profile in the three relative y locations ($y/b = -0.96$, $y/b = 0$, $y/b = 0.26$) along the transect at $x = 11.535$ m, for the leafless and foliated conditions. In the leafless condition (see *Figure 4.15a-b-c*), the vertical logarithmic profile (*Equation 32a*) describes very well the measured trends in the open channel ($y/b = -0.96$) and at the vegetation interface ($y/b = 0$). The RMS relative errors are low: 2.2% in the open channel and 2.0% at the vegetation interface. Within the vegetation ($y/b = 0.26$), there are some discrepancies that make the RMS relative error increased up to 15.0%, if the shear velocity used was calculated from the bed shear stress determined by *Equation 34a* (see Modelled_I curve in *Figure 4.15c*). If *Equation 36* was used, the RMS relative error was higher, about 33.6% (see Modelled curve in *Figure 4.15c*). In the foliated condition (see *Figure 4.15d-e-f*), *Equation 32a* describes quite well the vertical streamwise velocity above the bed. However, *Equation 32a* is not able to fit the reduction observed in the streamwise velocity close to the water free surface. For the streamwise velocity profiles in the open channel and at the vegetation interface the RMS relative errors are still under the threshold percentage of 10% (3.7% and 6.9%, respectively). Within the vegetation, the prediction is not reliable, in fact, RMS relative error is 49% if the shear velocity was calculated from the bed shear stress of *Equation 34a* (see Modelled_I curve in *Figure 4.15f*) and 40% if the shear velocity was determined by *Equation 36* (see Modelled curve in *Figure 4.15f*).

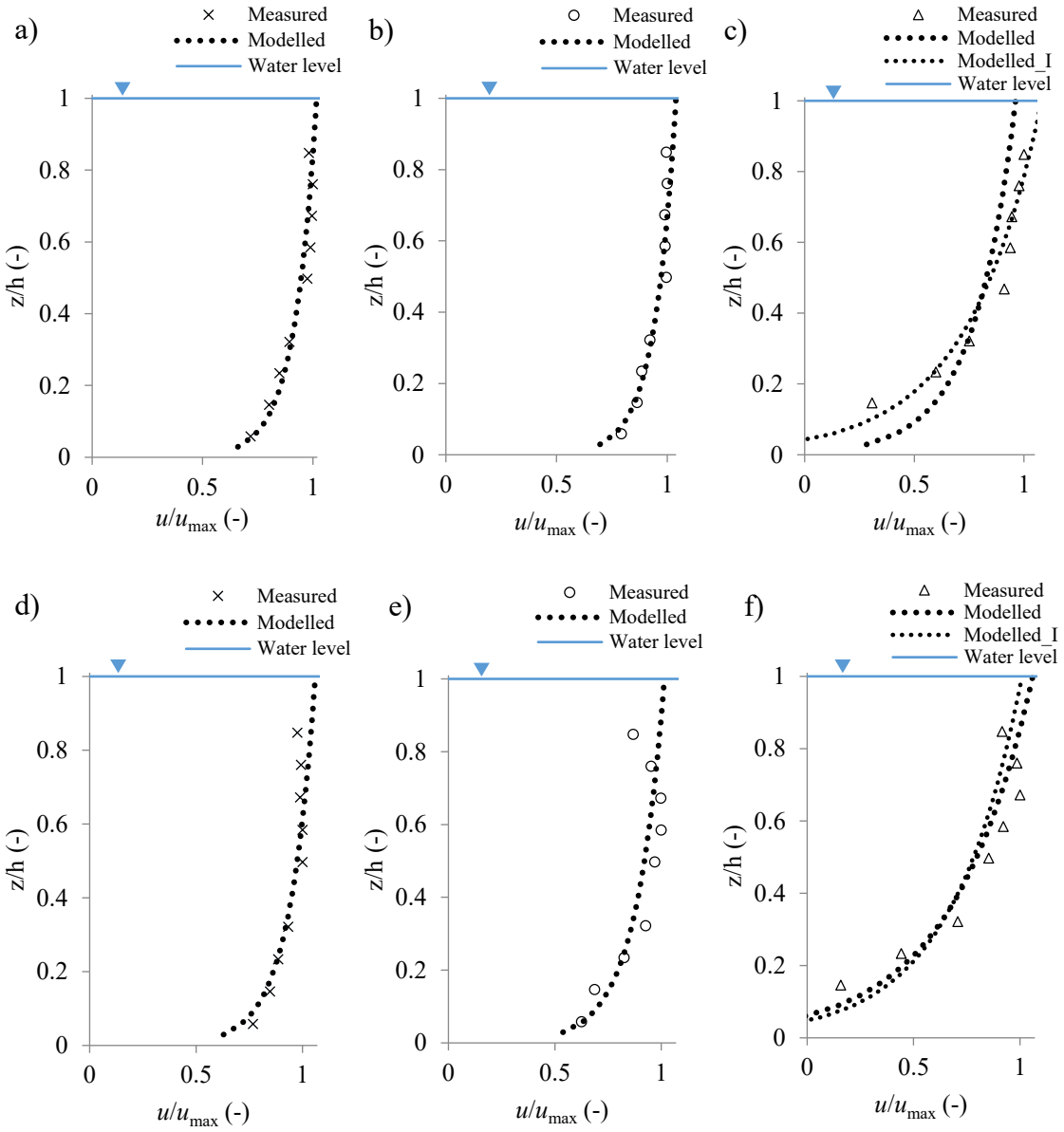

Figure 4.15: Normalized measured and modelled streamwise vertical velocity profiles in both vegetative conditions along the transect at $x = 11.535$ m. a) Represents the streamwise vertical velocity profiles at relative position $y/b = -0.96$ for the leafless condition, b) Represents the streamwise vertical velocity profiles at relative position $y/b = 0$ for the leafless condition, c) Represents the streamwise vertical velocity profiles at relative position $y/b = 0.26$ for the leafless condition, d) Represents the streamwise vertical velocity profiles at relative position $y/b = -0.96$ for the foliated condition, e) Represents the streamwise vertical velocity profiles at relative position $y/b = 0$ for the foliated condition, f) Represents the streamwise vertical velocity profiles at relative position $y/b = 0.26$ for the foliated condition. Whitin the vegetation (in *c)* and *f)*), Modelled_I represents the vertical streamwise velocity profile with the shear velocity determined by the *Equation 34a*.

Table 4.5 shows parameters and variables calculated and fitted using *Equation 32a* in *Section 3.3.1* for the vertical streamwise profiles in both vegetative conditions. The bed shear velocity (u_*), resulted from *Equation 36*, is higher for the foliated condition than in the leafless condition. Within the vegetation ($y/b = 0.26$), u_* decreases passing from leafless to leafy condition, using the calculation of the bed shear stress that takes into account the presence of emergent vegetation (*Equation 34a*). This reduction is in agreement with the decrease in bed shear stress due to the higher value of vegetation drag (see $C_D a$ and $C_D ah$ *Table 4.1* and *Table 4.2*), as Västilä & Järvelä (2017) pointed out. The

equivalent sand roughness (k_s) and the integration constant of the logarithm law (c) were fitted for each vertical streamwise profiles. k_s is always higher within the vegetation in comparison with the one in the open channel. The bottom grass mat, within the vegetation, makes the roughness (k_s) increased. Due to the direct relationship between k_s and the roughness height (z_0) (see *Equation 32b*), z_0 increases from the open channel to the vegetated patch.

Table 4.5: Experimental parameters and results for both vegetative conditions (leafless, foliated), for fitting of vertical streamwise velocity profiles.

Variable	Leafless condition				Foliated condition			
	y=-0.15m	y=0.07m	y=0.13m		y=-0.15m	y=0.07m	y=0.13m	
u_* (m/s)	0.029[a]	0.021[a]	0.035[a]	0.061[b]	0.040[a]	0.028[a]	0.055[a]	0.048[b]
k_s (m)	0.0005	0.001	0.229	0.026	0.0015	0.004	0.212	0.039
c (m/s)	0.295	0.290	0.452	0.195	0.381	0.257	0.403	0.185
z_0 (m)	0.0004	0.0009	0.19	0.024	0.0013	0.0036	0.179	0.034

[a] Shear velocity calculated by *Equation 36*.

[b] Shear velocity calculated by the shear bed stress of *Equation 34a*.

4.4.2 SSC Profiles

Two equations describing vertical profile of suspended solid concentration (SSC) were tested: Rouse's equation (*Equation 40*) and van Rijn's equation (*Equation 41*). At the vegetation interface, the sampling point closest to the bottom ($z/h = 0.15$) was neglected due to high value of SSC, likely affected by the presence of the grass mat in the sampling volume of the turbidity sensor.

Figure 4.16 shows normalized vertical profiles of measured and modelled suspended sediment concentration (SSC), divided by the maximum value of SSC in the profile (V_{SSCmax}). Two vertical profiles measured along the transect at $x = 11.535$ m, one in the open channel ($y/b = -0.96$) and one at the vegetation interface ($y/b = 0$), were considered for the comparison, for both the vegetative conditions. *Equations 40-41* were defined for unvegetated flow, and, for this reason, results for the fitting were better in the open channel than at the vegetation interface. Even if the RMS relative errors, for both the vegetative conditions, are higher than the threshold percentage (10%). *Equations 40-41* cannot be used to predict the SSC vertical profiles either in the open channel or at the vegetation interface, unlike to what assumed by Sharpe & James (2006) in their research on sedimentation processes in a partly vegetated channel using cylinder arrays.

In the leafless condition (*Figure 4.16a-b*), *Equations 40-41* deviate from the measured profile, only above the bed (until $z/h = 0.23$) the measured points are still predictable in reliable way. For the rest of the profile, both equations tend to underestimate the values of measured SSC. At the vegetation interface (*Figure 4.16b*), the measured vertical SSC profile is quite uniform from the free water surface to $z/h = 0.32$. *Equations 40-41* underestimated this trend and they do not describe this uniformity. The Root Mean Square

(RMS) relative error is about 55.2% for the Rouse's equation in both the relative positions along the y axis and about 54% and 53.2% for the van Rijn's equation in the open channel and at the vegetation interface. In the foliated condition (*Figure 4.16c-d*), the fitting of *Equations 40-41* follows the same trend of the ones resulted for the other vegetative condition. In the open channel (*Figure 4.16c*), *Equations 40-41* underestimate the measured values of SSC from the free water surface until $z/h = 0.2$ and predict well the points above the bed. The RMS relative errors are lower than the ones obtained for the leafless condition (35% for Rouse's equation and 32.7% for van Rijn's equation). At the vegetation interface (*Figure 4.16d*), *Equations 40-41* underestimate the sampling points close to the free water surface and overestimate measured SSC values close to the bed. The RMS relative errors are higher than the ones obtained in the leafless condition: 65.6% for the Rouse's equation and 63.7% for the van Rijn's equation.

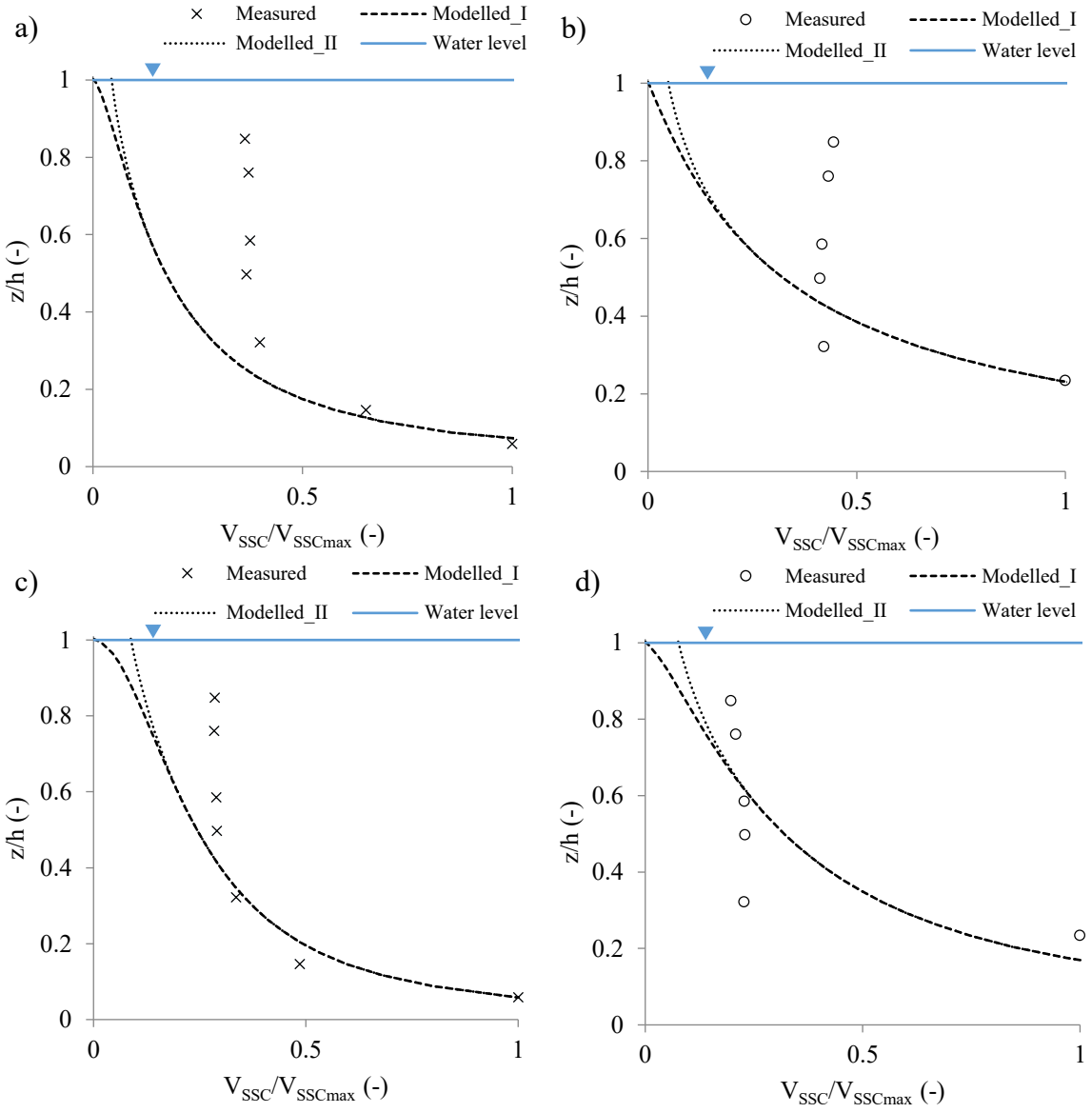

Figure 4.16: Normalized measured and modelled vertical suspended sediment concentration (SSC) profiles in both vegetative conditions along the cross-section at x=11.535 m. a) Represents the vertical SSC profiles at relative position $y/b = -0.96$ for the leafless condition, b) represents the vertical SSC profiles at relative position $y/b = 0$ for the leafless condition, c) Represents the vertical SSC profiles at relative position $y/b = -0.96$ for the foliated condition, d) Represents the vertical SSC profiles at relative position $y/b = 0$ for the foliated condition. Modelled_I represents the vertical SSC profile described using Rouse's equation (*Equation 40*), Modelled_II represents the vertical SSC described by van Rijn's equation (*Equation 41*).

Table 4.6 shows parameters and variables calculated and fitted using *Equations 40-41,* for the vertical SSC profiles in both vegetative conditions. Values of shear velocity (u_*) are the same used for testing the applicability of the vertical logarithmic profile (*Equation 32a*) for the vertical streamwise velocity (see *Table 4.5*). The reference SSC at the height α (C_α) resulted from the fitting, is very similar to measured value of SSC closest to the bed. In the non-linear fitting, initial values of C_α and α were the measured SSC value closest to the bed and the height from the bed where it was measured. Moving from leafless to leafy condition, C_α increases as the streamwise velocity in the open channel. Less particles can settle and their concentration is enhanced. The values of the reference height (α) are always higher at the vegetation interface ($y/b = 0$) than in the open channel ($y/b =$

-0.96), because of the presence of the grass mat characterizing the vegetated patch. α has values greater than the minimum threshold value ($0.01h$) assumed by van Rijn (1984) to avoid large errors and maintain a certain reliability in the prediction.

Table 4.6: Experimental parameters and results for both vegetative conditions (leafless, foliated), for vertical SSC profiles.

Variable	Leafless condition		Foliated condition	
	y=-0.15m	y=0.07m	y=-0.15m	y=0.07m
u_* (m/s)	0,029	0,021	0,040	0,028
C_α (V_{ssc})	0,289	0,170	0,302	0,468
α (m)	0,01	0,035	0,01	0,026

4.5 Uncertainty

Uncertainty can be linked to different types of sources such as resolution of sensor used (see *Section 3.1.1*), accuracy in data measurements, assumptions and simplifications of processes observed (see *Section 3.2-3.3*), propagation of errors in the pre-processing and in data analyses.

The accuracy for velocity and SSC measurements depends on the position of the sampling point along the vertical or transverse profile and on the vegetative condition. Higher errors occurred in the foliated condition due to the presence of the leaves entering the sampling volume of sensors. At the vegetation interface, fluctuations of measurements were the highest due to the presence of the shear mixing layer. In the open channel, errors were always lower compared to the ones detected within the vegetation. For streamwise velocity measurements, the standard deviation, calculated through the *Equation 21* ranged from ± 0.03 m/s to ± 0.08 m/s in the leafless condition and from ± 0.05 m/s to ± 0.15 m/s in the foliated condition. Errors in velocity measurements using ADV sensors, as noticed by Järvelä (2005), were caused by low signal-to-noise ratio (SNR), measuring time and imprecise orientation of the probe. During ADV measurements, SNR was taken into account setting an acceptable lower limit ($SNR > 15$) to guarantee good quality data. Instantaneous velocity measurements were collected for a period long enough (125 s) to detect velocity components and relative fluctuations. Sukhodolov & Sukhodolova (2010) used in their velocity measurements on field a sampling period of four times higher than the one considered in this study. In order to ensure a correct orientation of the probe, the ADV sensor was placed at a certain location in the beginning of the flume ($x = 3.1$ m, $y = -0.13$ m, $z = 0.095$ m) (see *Figure 3.3*) before starting velocity measurements, and the probe was orientated until getting a value of the velocity component along the y direction not exceeding a range of ± 0.2 cm/s. For the SSC measurements, the percentage of accuracy, calculated as standard deviation (*Equation 21*) divided by the average value (*Equation 20*), ranged from ± 2 % to ± 5 % in the leafless condition and from ± 9 % to ± 17 % in the foliated condition. The difference in the accuracy was also due to the use of different sensors (see *Section 3.1.1*). The rough errors were likely due to the sediment

feeding rate not properly constant and to the different accuracy in cleaning the flume from the sediment after each experiment. A reference concentration of suspended sediment (see *Section 3.1.3*) was always collected in the beginning of the experiments, in order to detect the initial value of SSC to compare SSC measurements performed in different experiments. The accuracy of net deposition within the vegetated patch, was calculated as standard deviation (*Equation 21*) and reported in *Table 4.3*. Depending on the location of the sampling points, the standard deviation ranged from $\pm 1.11 * 10^{-4}$ g/s to $\pm 6.94 * 10^{-4}$ g/s. Measurements performed next to the vegetated interface were affected by a larger error, due to discrepancies in how grass mat strips were attached to the bottom bed. In some experiments the strips were about half of centimetre lifted, letting sediments being trapped under them.

The artificial natural-like vegetation and the grass mat were to some extent damaged a little damaged by the water flow force. To maintain the same density and vegetation properties, the state and shape of leaves were checked from an experiment to the other one and the damaged plants were substituted. In the beginning of each experiment, the hydraulic conditions were set up carefully, modifying the slope and the weir. The water level was monitored automatically by six pressure sensors located along the bottom of the flume and manually using the needle.

In the test of applicability of theoretical and empirical relationships, the errors coming from the non-linear regression were affected by the number of sampling points used for the fitting. Especially for the vertical profiles of streamwise velocity and SSC, the measured points were not enough to guarantee a reliable prediction of the unknown variables. The input parameters used in the equations for the comparison (see *Figure 3.11*) were calculated from the measured values. The error propagation affected the calculation of these parameters and influenced the accuracy of the non-linear regression and, consequently, the Root-Mean-Square (RMS) relative errors obtained by the comparison between the predicted and measured profiles.

5. Conclusion

This experimental research aimed at improving the understanding on turbulent flow, sediment transport and net deposition in partly vegetated flows. One side of the bottom of the flume was covered by low artificial understory grass mat and emergent artificial flexible natural-like plants. In the fully developed flow region, transverse and vertical profiles were measured using different sensors. Measurements were pre-processed and analysed, testing theoretical and empirical relationships from literature.

The vegetation interacted with the water flows, altering the flow field, the transport of suspended fine sediment and the net deposition compared to the unvegetated part of the cross-sections. Results showed that the average streamwise velocity decreased within the vegetated patch and increased along the open channel. The streamwise velocity gradient was enhanced when the plant density increased, passing from leafless to foliated condition. Across the interface between the vegetation and the main channel, the presence of the mixing layer generated complex phenomena in which the turbulence is the main player. Within the foliated vegetation, suspended sediment concentration (SSC) was characterized by a decrease due to the higher reduction in streamwise velocity and increase in the net deposition. In this vegetative condition, turbulent stresses declined rapidly and the mechanic dispersion was the main sediment transport process. In the leafless condition, the SSC gradient between open channel and the patch was reduced and turbulence at the stem scale played the main role in fine sediment transport. Within the leafless vegetation, vertical SSC profiles showed high variability and the net deposition was reduced. The net deposition was enhanced at the vegetation interface due to the increase in transverse fine sediment transport, strictly linked to the high momentum transfer in the mixing layer.

The use of theoretical and empirical formulae defined for unvegetated flow or partly vegetated flow from laboratory or field experiments is not so reliable for predicting the flow field and fine sediment transport under the presently examined conditions. Deviations in results were mainly due to properties and the pattern of vegetation used in these experiments, different from common vegetative conditions of earlier research activities characterized by rigid plant elements with very high density. The flexibility and the morphology of the artificial emergent woody plants allowed a natural-like reconfiguration and movement of stems and leaves under the water flow, while the density represented the natural density of riverine shrubs and bushes. The test applicability revealed that, in the leafless condition, predictions on streamwise velocity profiles were still valid for the open channel and, with a small error, within the vegetation. The leafless condition is similar to the vegetative condition used in literature using cylinder-shape elements. In the foliated condition, deviations from measured profiles increased, making the prediction of streamwise velocity within the vegetated patch harder and more unreliable. The predictions on vertical SSC profiles were completely unreliable for both vegetative conditions in the open channel and at the vegetation interface.

As leafless and foliated conditions resemble seasonal changes in the riverine vegetation lifecycle, the present findings and observations can be useful to predict and determine a good maintenance of channels to control nutrient transport and water quality. Overall, future investigations are needed in order to have a clear understanding of the yet unknown water flow-vegetation-sediment interactions in a controlled environment, where the main variables can be easily determined or measured. For example, by changing the setting of hydraulic conditions (e.g. relative submergence ratio), density of the vegetation, sediment supply or particle size distribution.

References

Aberle, J., & Järvelä, J. (2015). Hydrodynamics of Vegetated Channels. In P. Rowiński, & A. Radecki-Pawlik , *Rivers – Physical, Fluvial and Environmental Processes* (pp. 519-541). GeoPlanet: Earth and Planetary Sciences. Springer, Cham.

Abt, S., Clary, W., & Thornton, C. (1994). Sediment deposition and entrapment in vegetated streambeds. *Journal of Irrigation and Drainage Engineering, 120(6)*, 1098-1111.

Albayrak, I., Nikora, V., Miler, O., & O'Hare, M. (2014). Flow–plant interactions at leaf, stem and shoot scales: drag, turbulence, and biomechanics. *Aquatic Sciences, 76*, 269–294.

Bal, K., Struyf, E., Vereecken, H., Viaene, P., De Doncker, L., de Deckere, E., . . . Meire, P. (2011). How do macrophyte distribution patterns affect hydraulic resistances? *Ecological Engineering, 37*, 529–533.

Bennett, S., Pirim, T., & Barkdoll, B. (2002). Using simulated emergent vegetation to alter stream flow direction within a straight experimental channel. *Geomorphology, 44(1–2)*, 115–126.

Carollo, F., Ferro, V., & Termini, D. (2002). Flow Velocity Measurements in Vegetated Channels. *Journal of Hydraulic Engineering, 128(7)*, 664-673.

Celik, A., Diplas, P., Dancey, C., & Valyrakis, M. (2010). Impulse and particle dislodgement under turbulent flow conditions. *Physics of Fluids, 22*, 046601.

Chen, Z., Ortiz, A., Zong, L., & Nepf, H. (2012). The wake structure behind a porous obstruction and its implications for deposition near a finite patch of emergent vegetation. *Water Resources Research, 48*, W09517.

CSI. (2008). *OBS-3+ and OBS300 Suspended Solids and Turbidity Monitors: Instruction manual.* Campbell Scientific, Inc.

Defina, A., & Bixio, A. (2005). Mean flow and turbulence in vegetated open channel flow. *Water Resources Research, 41*, W07006.

Dietrich, W. (1982). Settling velocity of natural particles. *Water Resources Research, 18(6)*, 1615–1626.

Dunn, C., Lopez, F., & Garcia, M. (1996). Mean flow and turbulence in a laboratory channel with simulated vegetation. *Hydraulic Engineering Series, 51*.

Elliott, A. (2000). Settling of fine sediment in a channel with emergent vegetation. *Journal of Hydraulic Engineering, 126*, 570-577.

Folkard, A. (2011). Vegetated flows in their environmental context: a review. In *Proceedings of the Institution of Civil Engineers - Engineering and Computational Mechanics 164(EM1)* (pp. 3-24).

Ghisalberti, M., & Nepf, H. (2002). Mixing layers and coherent structures in vegetated aquatic flows. *Journal of Geophysical Research, Vol. 107*.

Goring, D., & Nikora, V. (2002). Despiking acoustic Doppler velocimeter data. *Journal of Hydraulic Engineering, 128(1)*, 117–126.

Grace, J. (1986). Contacting modes and behaviour classification of gas-solid and other two-phase suspensions. *Canadian Journal of Chemical Engineering, Vol. 64*, 353-363.

Graf, W. (1971). *Hydraulics of Sediment Transport.* New York: McGraw-Hill.

Graf, W. (1998). *Fluvial Hydraulics: Flow and Transport Processes in Channels of Simple Geometry.* Chichester: John Wiley & Sons Ltd.

Ishibashi,, I., & Hazarika, H. (2010). *Soil Mechanics Fundamentals.* CRC Press.

Jalonen, J., Järvelä, J., & Aberle, J. (2013). Leaf area index as vegetation density measure for hydraulic analyses. *Journal of Hydraulic Engineering, 139(5)*, 461–469.

Jalonen, J., Järvelä, J., Koivusalo, H., & Hyyppä, H. (2014). Deriving floodplain topography and vegetation characteristics for hydraulic engineering applications by means of terrestrial laser scanning. *Journal of Hydraulic Engineering, 140(11)*.

James, C., Jordanova, A., & Nicolson, C. (2002). Flume experiments and modelling of flow-sediment-vegetation interactions. In F. Dyer, M. Thoms, & J. Olley, *Structure, Function and Management Implications of Fluvial Sedimentary Systems* (pp. 3–9). Wallingford: IAHS Press.

Järvelä, J. (2002). Flow resistance of flexible and stiff vegetation: A flume study with natural plants. *Journal of Hydrology, 269(1–2)*, 44–54.

Järvelä, J. (2005). Effect of submerged flexible vegetation on flow structure and resistance. *Journal of Hydrology, 307*, 233–241.

Jesson, M., Bridgeman, J., & Sterling, M. (2015). Novel software developments for the automated post-processing of high volumes of velocity time-series. *Advances in Engineering Software, 89*, 36-42.

Jimenez, J., Madsen, O., & ASCE, M. (2003). Formula to Estimate Settling Velocity of Natural Sediments. *Journal of Waterway, Port, Coastal, Ocean Engineering, 129(2)*, 70-78.

Kouwen, N. (1998). Field estimation of the biomechanical properties of grass. *Journal of Hydraulic Research, 26(5)*, 559-568.

Kouwen, N., & Unny, T. (1973). Flexible roughness in open channels. *Journal of the Hydraulic Division, ASCE, 99*, 713–728.

Kouwen, N., Unny, T., & Hill, H. (1969). Flow retardance in vegetated channels. *Journal of the Hydraulic Division, ASCE, 95(IR2)*, 329–342.

Lightbody, A., & Nepf, H. (2006). Prediction of velocity profiles and longitudinal dispersion in emergent salt marsh vegetation. *Limnology and Oceanography, 51(1)*, 218–228.

Łoboda, A., Przyborowski, Ł., Karpinski, M., Bialik, R., & Nikora, V. (2018). Biomechanical properties of aquatic plants: The effect of test conditions. *Limnology and Oceanography: Methods 16*, 222-236.

Lopez, F., & Garcia, M. (1998). Open-channel flow through simulated vegetation: Suspended sediment transport modeling. *Water Resources Research, 34 (9)*, 2341-2352.

Luhar, M., & Nepf, H. (2011). Flow-induced reconfiguration of buoyant and flexible aquatic vegetation. *Limnology and Oceanography, 56(6)*, 2003–2017.

Luhar, M., & Nepf, H. (2013). From the blade scale to the reach scale: A characterization of aquatic vegetative drag. *Advances in Water Resources, 51*, 305–316.

Luhar, M., Rominger, J., & Nepf, H. (2008). Interaction between flow, transport and vegetation spatial structure. *Environmental Fluid Mechanics, 8*, 423–439.

Ma, G. (2014). Modeling wave damping and sediment transport within a patch of vegetation. *Proceedings of 34th International Conference on Coastal Engineering, ICCE2014.* Soul, Korea.

McAnally, W., & Mehta, A. (2002). Signifigance of aggregation of fine sediment particles in their deposition. *Estuarine, Coastal and Shelf Science, 54(4)*, 643–653.

Miler, O., Nikora, V., Albayrak, I., & O'Hare, M. (2014). Biomechanical properties and morphological characteristics of lake and river plants: Implications for adaptations to flow conditions. *Aquatic Science, 76*, 465–481.

Nepf, H. M. (1999). Drag, turbulence, and diffusion in flow through emergent vegetation. *Water Resources Research, 35(2)*, 479-489.

Nepf, H. M. (2012a). Flow and Transport in Regions with Aquatic Vegetation. *Annual Review of Fluid Mechanics, 44*, 123–142.

Nepf, H. M. (2012b). Hydrodynamics of vegetated channels. *Journal of Hydraulic Research Vol. 50, No. 3*, 262–279.

Nepf, H., Rominger, J., & Zong, L. (2013). Coherent Flow Structures in Vegetated Channels. In J. Venditti, J. Best, M. Church, & R. J. Hardy, *Coherent Flow Structures at Earth's Surface* (pp. 135-147). JohnWiley & Sons, Ltd.

Nezu, I., & Okamoto, T.-a. (2013). Hydraulics of Vegetated Canopies. In H. Shermal Fernando, *Handbook of Environmental Fluid Dynamics, Volume One* (pp. 285-309). CRC Press/Taylor & Francis Group, LLC.

Nikora, N., Nikora, V., & O'Donoghue, T. (2013). Velocity Profiles in Vegetated Open-Channel Flows: Combined Effects of Multiple Mechanisms. *Journal of Hydraulic Engineering, 139(10)*, 1021-1032.

Nikora, V. (2010). Hydrodynamics of aquatic ecosystems: an interface between ecology, biomechanics and environmental fluid mechanics. *River Research and Applications, 26(4)*, 367–384.

Nikora, V., Cameron, S., Albayrak, I., Miler, O., Nikora, N., Siniscalchi, F., . . . O'Hare, M. (2012). Flow-biota interactions in aquatic systems: Scales, mechanisms, and challenges. In W. Rodi, & M. Uhlmann, *Environmental fluid mechanics : Memorial Volume in honour of Prof. Gerhard H. Jirka* (pp. 217-235). CRC Press.

Nikora, V., Goring, D., & Griffiths, G. (2001). Spatially Averaged Open-Channel Flow over Rough Bed. *Journal of Hydraulic Engineering, 127(2)*, 123-133.

Nikora, V., McEwan, I., McLean, S., Coleman, S., Pokrajac, D., & Walters, R. (2007a). Double-Averaging Concept for Rough-Bed Open-Channel and Overland Flows: Theoretical Background. *Journal of Hydraulic Engineering, 133(8)*, 873-883.

Nikora, V., McLean, S., Coleman, S., Pokrajac, D., McEwan, I., Campbell, L., . . . Koll, K. (2007b). Double-Averaging Concept for Rough-Bed Open-Channel and Overland Flows: Applications. *Journal of Hydraulic Engineering, 133(8)*, 884-895.

Nortek AS. (2009). *Vectrino Velocimeter: User Guide.*

Observation Instruments. (2015). *ANALITE NEP-5000 Turbidity Sensor Multiple Output Auto-Ranging.* Scoresby.

Ortiz, A., Ashton, A., & Nepf, H. (2013). Mean and turbulent velocity fields near rigid and flexible plants and the implications for deposition. *Journal of Geophysical Research, 118*, 2585–2599.

Parsheh, M., Sotiropoulos, F., & Porté-Agel, F. (2010). Estimation of Power Spectra of Acoustic-Doppler Velocimetry Data Contaminated with Intermittent Spikes. *Journal of Hydraulic Engineering, 136(6)*, 368-378.

Plew, D. R. (2011). Depth-Averaged Drag Coefficient for Modeling Flow through. *Journal of Hydraulic Engineering, 137(2)*, 234-247.

Poggi, D., Katul, G., & Albertson, J. (2004). A note on the contribution of dispersive fluxes to momentum transfer within canopies. *Boundary-Layer Meteorology, 111(3)*, 615–621.

Rominger, J., & Nepf, H. (2011). Flow adjustment and interior flow associated with a rectangular porous obstruction. *Journal of Fluid Mechanics, 680*, 636–659.

Schmid, B., Stephan, U., & Hengl, M. (2005). Sediment deposition in constructed wetland ponds with emergent vegetation: laboratory study and mathematical model. *Water Science and Technology, 51(9)*, 307–314.

Sharpe, R., & James, C. (2006). Deposition of sediment from suspension in emergent vegetation. *Water SA, 32(2)*, 211-218.

Sibelco Benelux. (2009). *Technical Data Silica Sand S50-S60-S80-S90.* Dessel.

Siniscalchi, F., Nikora, V., & Aberle, J. (2012). Plant patch hydrodynamics in streams: Mean flow, turbulence, and drag forces. *Water Resources Research, 48*, W01513.

Sukhodolov, A., & Sukhodolova, T. (2010). Case Study: Effect of Submerged Aquatic Plants on Turbulence Structure in a Lowland River. *Journal of Hydraulic Engineering, 136(7)*, 434-446.

Sun, R., Xiao, H., & Sun, H. (2018). Investigating the Settling Dynamics of Cohesive Silt Particles With Particle-Resolving Simulations. *Advances in Water Resources, 111*, 406–422.

Tanino, Y., & Nepf, H. (2008). Lateral dispersion in random cylinder arrays at high Reynolds number. *Journal of Fluid Mechanics, 600*, 39–71.

Turton, R., & Levenspiel, O. (1986). A short note on the drag correlation for spheres. *Powder Technology, 47*, 83-86.

van Prooijen, B., Battjes, J., & Uijttewaal, W. (2005). Momentum Exchange in Straight Uniform Compound Channel Flow. *Journal of Hydraulic Engineering, 131(3)*, 175-183.

van Rijn, L. (1984). Sediment Transport, Part II: Suspended Load Transport. *Journal of Hydraulic Engineering, 110(11)*, 1613-1641.

Vargas-Luna, A., Crosato, A., & Uijttewaal, W. (2015). Effects of vegetation on flow and sediment transport: comparative analyses and validation of predicting models. *Earth Surface Processes and Landforms, 40*, 157–176.

Västilä, K. (2015). *Flow–plant–sediment interactions: Vegetative resistance modeling and cohesive sediment processes.* Aalto University.

Västilä, K., & Järvelä, J. (2017). Characterizing natural riparian vegetation for modeling of flow and suspended sediment transport. *Journal of Soils and Sediments*.

Västilä, K., Järvelä, J., & Koivusalo, H. (2016). Flow–Vegetation–Sediment Interaction in a Cohesive Compound Channel. *Journal of Hydraulic Engineering, 142(1)*, 04015034.

Wahl, T. (2003). Discussion of despiking acoustic Doppler velocimeter data. *Journal of Hydraulic Engineering, 129(6)*, 484–487.

White, B., & Nepf, H. (2007). Shear instability and coherent structures in shallow flow adjacent to a porous layer. *Journal of Fluid Mechanics, 593*, 1–32.

White, B., & Nepf, H. (2008). A vortex-based model of velocity and shear stress in a partially vegetated shallow channel. *Water Resources Research, 44*.

Wilson, C. (2007). Flow resistance models for flexible submerged. *Journal of Hydrology, 342*, 213– 222.

Wilson, K. C., Addie, G. R., Sellgren, A., & Clift, R. (2006). *Slurry Transport Using Centrifugal Pumps.* Springer US.

Wu, F.-C., Shen, H., & Chou, Y.-J. (1999). Variation of roughness coefficients for unsubmerged and submerged vegetation. *ASCE Journal of Hydraulic Engineering, 125 (9)*, 934–942.

Wu, W., Shields Jr., F., Bennett, S., & Wang, S. (2005). A depth-averaged two-dimensional model for flow, sediment transport, and bed topography in curved channels with riparian vegetation. *Water Resources Research, 41*, W03015.

Zheng, J., Li, R.-j., Feng, Q., & Lu, S.-s. (2013). Vertical profiles of fluid velocity and suspended sediment concentration in nearshore. *International Journal of Sediment Research, 28*, 406-412.

Zong, L., & Nepf, H. (2010). Flow and deposition in and around a finite patch of vegetation. *Geomorphology, 116*, 363–372.

Zong, L., & Nepf, H. (2011). Spatial distribution of deposition within a patch of vegetation. *Water Resources Research, 47*, W03516.